

BARRIER RESONANCES AND CHEMICAL REACTIVITY

RONALD S. FRIEDMAN* AND DONALD G. TRUHLAR†

Abstract. We survey the phenomenology of broad and overlapping resonances in the scattering theory of molecular collisions. We first discuss examples of resonances encountered in molecular collisions that are not described by the well known isolated narrow resonance formulae; nevertheless certain regularities are observed. We emphasize (i) the relationship between the total resonance width and the sum of the partial widths and (ii) the comparison of trapped-state resonances to barrier resonances, especially from the point of view of the change in background (direct) scattering over the width of the resonance. We then focus on quantal scattering by one-dimensional potential energy functions to provide further insight into the nature of barrier resonances, which are also called transition states. In studies of symmetric and unsymmetric potential functions, we show that reaction thresholds associated with barriers are associated with poles of the scattering matrix; i.e., chemical reaction thresholds are resonances. As the parameters of the potential function are varied, we follow the "trajectory" of the poles in the complex energy plane and examine the connection between barrier resonances and conventional resonances associated with wells between barriers. Resonances are further characterized by considering the relationship between the resonance width and the reactive delay time.

Key words. chemical reactions, poles of the scattering matrix, resonances, spectroscopy of the transition state

AMS(MOS) subject classifications. 81U10, 81U05, 81U20

1. Introduction. "Probably the most striking phenomenon in the whole range of scattering experiments is the resonance. Resonances are observed in atomic, nuclear and particle physics. In their simplest form they lead to sharp peaks in the total cross section as a function of energy . . . There are many different theoretical approaches to the resonance phenomenon, all of them having in common that the sharp variation of the cross section . . . is in some way related to the existence of a *nearly bound state* of the projectile-target system . . ." [1].

Thus resonance states are metastable states, and such states have a much richer phenomenology than true bound states. The present contribution to the interdisciplinary workshop will focus on metastable states and resonance phenomena in chemically reactive molecular scattering processes that raise interesting and incompletely understood questions about correlating observed phenomena with the analytic structure of the scattering matrix. The chapter includes examples of specific case studies and relevant background. References are illustrative without attempting to give a complete survey of the literature.

* Department of Chemistry, Indiana University Purdue University Fort Wayne, Fort Wayne, IN 46805-1499.

† Department of Chemistry and Supercomputer Institute, University of Minnesota, Minneapolis, MN 55455-0431.

1.1. Trapped-state and barrier resonances. Metastable states in quantum mechanics are usually associated with quasibound states located in a potential well which may be between barriers or behind a barrier. The barrier separating the resonance state from the dissociative continuum may be in the potential energy or in an effective potential curve (potential energy plus centrifugal potential); in such cases the resonance is called a "shape resonance" or "single-particle resonance." Alternatively, the barrier may be associated with slow energy transfer from internal modes of one of the collision partners to the dissociative mode, i.e., to the collision coordinate; such resonances are variously known as core excited [1], internal-excitation [2], target excited [3], or Feshbach [4,5] resonances. The finite lifetime associated with the metastable state can manifest itself in a time delay for the scattering phenomenon (relative to the free particle motion in the absence of a potential) and in rapid variations in cross sections and transition probabilities. We refer to such metastable states as "trapped-state resonances."

However, metastability is not limited to states located "behind barriers". It is well known in *classical* mechanics that a potential *maximum* is associated with metastability at the energy of the maximum; passage over the barrier incurs a time delay due to the system slowing down *as it crosses* the barrier top. There should be, and in fact is, an analogue in *quantum* mechanics [6]. Quantum mechanically, barrier passage is also associated with a time delay, manifested as an increasing phase in elements of the scattering (S) matrix (relative to the background phase, i.e., the phase itself or show an increase or a less rapid decrease in the vicinity of the barrier) [3,7-9]. The time delays associated with barrier passage have been shown, as will be discussed below, to be associated with metastable states [10-12], which we will refer to as "barrier resonances."

Trapped-state and barrier resonances share one very important feature: they are both "resonances," which we define, using the most fundamental definition we know [1a,13-18], as observable, energy-localized manifestations of poles of the scattering matrix (S matrix) at complex (resonance) energies z_α given by

$$(1.1) \quad z_\alpha = \varepsilon_\alpha - i\Gamma_\alpha/2$$

The index α (a collection of quantum numbers) labels the resonance, ε_α is the real part of the resonance energy and Γ is the (total) resonance width. That there is no distinction *in kind* between barrier and trapped-state resonances has been demonstrated in one-dimensional scattering studies [11,12] in which it has been shown that by continuously varying the form of the potential barrier function, a barrier resonance may be transformed into a trapped-state resonance and vice versa. In fact, in both the one-dimensional studies as well as three-dimensional, multiparticle reactive scattering work [19-21] we have found that a resonance need not be uniquely described as either a trapped-state or a barrier resonance but instead may

partake of the characters of both. Nonetheless, although the classification of a pole of \mathbf{S} as a barrier or trapped-state resonance is not always unambiguous, the distinction between the two types of resonances is useful, just as the subdivision [2,4] of trapped-state resonances into internal-excitation and shape resonances has proved useful in a wide variety of contexts. Trapped-state resonances in general tend to be associated with longer time delays and narrower widths than barrier resonances.

1.2. Isolated narrow resonances. The molecular collisions under consideration in this chapter are invariant under time reversal and, as a consequence, phases can be chosen so that the scattering matrix is symmetric [22], and we will do so. In the vicinity of an isolated resonance, the scattering matrix element $S_{n'n}$, where $n(n')$ denotes the set of quantum numbers for the initial (final) channel, can be written [1a,15,23-26]

$$(1.2) \quad S_{n'n}(E) = S_{n'n}^b(E) - i \frac{\gamma_{\alpha n'} \gamma_{\alpha n}}{E - z_\alpha}$$

where z_α is given by eqn (1.1), $S_{n'n}^b(E)$ is the nonresonant background contribution to the scattering matrix element, E is the total energy, and $\gamma_{\alpha n'}$ is the partial width amplitude for channel n' . We immediately see that at the complex resonance energy z_α , there is a pole in the \mathbf{S} matrix.

The total width Γ_α of eqn (1.1) is directly related to the rate constant k_α for the unimolecular decay of the resonance state [27,28]

$$(1.3) \quad k_\alpha = \Gamma_\alpha / \hbar$$

where \hbar is Planck's constant (h) divided by 2π . The rate constant itself is defined by

$$(1.4) \quad dC_\alpha/dt = -k_\alpha C_\alpha$$

where C_α is the number density of state α . Defining the "lifetime" τ_α as the reciprocal of the rate constant yields

$$(1.5) \quad \tau_\alpha = \hbar / \Gamma_\alpha$$

The "partial width" $\Gamma_{\alpha n'}$ for leaving the metastable resonance to go into final channel n' (or for entering it from channel n') is given by $|\gamma_{\alpha n'}|^2$. (It can also be defined using a golden-rule type of formula in terms of properly normalized resonance wave functions [29].)

For an isolated, narrow resonance (INR) one can show that [1a,15,23-29]

$$(1.6) \quad \sum_n \Gamma_{\alpha n} = \Gamma_\alpha$$

where the sum extends over all open (i.e., energetically accessible) channels. The partial width $\Gamma_{\alpha j}$ controls the rate constant $k_{\alpha j}$ of unimolecular decay

of the resonance α into a specific (initial or final) state j just as the total width Γ_α controls the total decay rate k_α . In particular [29],

$$(1.7) \quad k_{\alpha j} = \Gamma_{\alpha j} / \hbar$$

Using eqn (1.2) and neglecting the background contribution $S_{n'n}^b$ and the interference between the background and resonant contributions, we see that the channel-to-channel transition probability $P_{n \rightarrow n'}$, to the extent that it is controlled by resonance α , is given by

$$(1.8) \quad |S_{n'n}|^2 = \frac{\Gamma_\alpha^2}{(E - \varepsilon_\alpha)^2 + \Gamma_\alpha^2/4} P_{\alpha n} P_{\alpha n'}$$

where

$$(1.9) \quad P_{\alpha j} = \Gamma_{\alpha j} / \Gamma_\alpha$$

We see that pure resonant scattering is statistical with branching ratios entirely governed by the partial widths. In other words, the decay of the resonance is independent of its mode of formation. This property obviously follows from the factorization of the residue in eqn (1.2).

Since the scattering matrix is unitary and symmetric, it can be diagonalized by a real, orthogonal matrix \mathbf{B} :

$$(1.10) \quad S_{n'n} = \sum_m B_{n'm} e^{2i\Delta_m} B_{mn}$$

where Δ_m are called eigenphase shifts or the eigenphases. The eigenphase sum Δ is given by

$$(1.11) \quad \Delta = \sum_m \Delta_m$$

For an isolated narrow resonance, the eigenphase sum follows the multi-channel Breit-Wigner formula [30]

$$(1.12) \quad \Delta(E) = \Delta^b(E) + \arctan \frac{\Gamma_\alpha}{2(\varepsilon_\alpha - E)}$$

where Δ^b is the background contribution. If the background contribution is negligible, the eigenphase sum increases by exactly π as one transverses the real energy ε_α [31]. The eigenphase sum can be calculated by diagonalizing \mathbf{S} and using eqn (1.11) or more simply by using

$$(1.13) \quad \exp(2i\Delta) = \det \mathbf{S}$$

A resonance may also be characterized in terms of a channel-to-channel delay time $\Delta t_{nn'}$, which is the time difference between the injection of a

pulse in initial channel n and the appearance of a pulse in final channel n' , relative to the same delay time in the absence of a potential. In general, the delay time is defined by [3,11,12,32,33]

$$(1.14) \quad \Delta t_{nn'} = \text{Im} \left(\hbar (S_{n'n})^{-1} \frac{dS_{n'n}}{dE} \right)$$

or equivalently

$$(1.15) \quad \Delta t_{nn'} = \hbar \frac{d}{dE} \arg S_{n'n}(E)$$

The scattered particle will experience a delay time at real energies in the proximity of ε_α which is expected to be large if the resonance width is small. In particular, if the resonance is an INR, then from eqns (1.2) and (1.14) and the assumption that $S_{n'n}^b$ is negligible, one can easily show that $\Delta t_{nn'}$ will have a maximum at $E = \varepsilon_\alpha$, at which

$$(1.16) \quad \Delta t_{nn'} = 2\hbar/\Gamma_\alpha$$

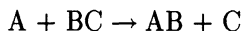
Note that this result is independent of n and n' in this limit. The factor of two difference between eqns (1.5) and (1.16) is due to the fact that unimolecular decay may be considered a half collision, whereas eqn (1.16) has contributions from both the incoming and outgoing segments of the collision.

1.3. Overlapping and broad resonances. All of the above INR formulas are expected to hold very well for INRs except [34] where they are close to an energetic threshold. For example these formulas apply extremely well to the resonances observed in a quantum mechanical study of nonreactive atom-molecule scattering by Ashton et al. [35]. However, more generally, resonances encountered in molecular collisions are *not* well described by all of the INR formulas. In this section, we briefly review some literature on overlapping and broad resonances, and we present a few relevant examples from the literature in which partial widths of scattering resonances were determined.

Formal analysis of overlapping resonances is much more scarce than for isolated resonances. In paper III of his well known series on a unified theory of nuclear reactions, Feschbach [36] provided a general treatment of overlapping resonances in terms of complex effective potentials, but this analysis has been much less widely used than his analysis in paper II [5] of isolated resonances. The photoabsorption line shape in the case of *independent* overlapping resonances was considered by Shore [37]. The question of degenerate resonances and avoided resonance intersections has been treated recently by Mondragón and Hernández [38]. Desouter-Lecomte and coworkers [39] also discussed the intersection of two or more nearby resonance poles. In general, overlapping of resonances refers to their having real parts that are the same within approximately the sum of their widths,

whereas an intersection would be where both their real and imaginary parts are equal.

Schwenke and Truhlar [27] characterized a total of 14 trapped-state resonances for several different collinear reactions



treated as three bodies constrained to the z axis and interacting by an analytic potential energy surfaces. (After the center of mass motion has been removed from the collinear problem, two mathematical dimensions remain, which may, for example, be taken as the A-to-B and B-to-C distances.) For each resonance, z_α was evaluated and a full set of partial widths determined. In each case, the eigenphase sum Δ followed the INR formula (1.12) very well, and no special difficulties were encountered in performing fits to obtain ε_α and Γ_α . The background Δ^b was represented as a polynomial in energy. With the location of the scattering resonance determined, a fit of each scattering matrix element at real energies near ε_α to eqn (1.2) resulted in the evaluation of the residue. When we take account of the symmetry of \mathbf{S} , there are $(N^2 + N)/2$ residues; but there are only N partial width amplitudes. Thus least square fitting of resonance parameters (as well as background) was used to extract best-fit values of the partial widths.

The ratio

$$(1.17) \quad q_\alpha = \frac{\sum_n \Gamma_{\alpha n}}{\Gamma_\alpha}$$

was then computed to see how well INR formula (1.6) was followed. For all 14 resonances, the ratio was less than unity, and for 12 of them it was significantly less, falling in the range from 0.23 to 0.76; for the remaining two resonances, q_α was 0.99 and 0.98. The wider resonances showed the greatest deviation from unity. The conclusion reached in this study was that most of the reactive resonances are not narrow enough to be characterized as INRs.

The significance of q_α differing from unity has been discussed from several different points of view in the literature. Lane and Thomas [23] noted that partial widths smaller than the INR limits will result when the resonance scattering wavefunction has large amplitude in the region external to the Wigner R matrix [40] boundary. Weidenmüller, using analytic S matrix theory, showed that even when a resonance is isolated enough that eqn (1.12) is followed, q_α need not equal unity if the resonance is not narrow enough [25]. Weidenmüller [25] presented numerical results showing $q_\alpha \leq 1$; he showed that even when $q_\alpha \neq 1$, the sum of the eigenphases increases by π at a resonance and the resonant part of the S matrix still factorizes. Further analyses [24,29] have given explicit formal expressions for this ratio using correctly normalized resonance wavefunctions. Consistent with all these works is that q_α may deviate more significantly from 1

for the wider resonances. Of course when $q_\alpha \neq 1$, it would appear that the sum of the specific unimolecular rate constants does not equal the total unimolecular rate constant. The only satisfactory conclusion is that when $q_\alpha \neq 1$, the decay process is intrinsically nonexponential and the rate constants are not all well defined. Since the decay cannot be exponential at $t = 0$ [17], a short-lived resonance may have effectively decayed away before the exponential law has time to manifest itself. Examples of short-lived decaying states for which there is no time for the exponential law to manifest itself have been discussed by Beck and Nussenzweig [41]. The exponential decay law has been discussed by Desouter-Lecomte and Culot in the context of overlapping resonances; they concluded that in the statistical regime of highly overlapped resonances, the decay of a metastable system will be nonexponential, and they discussed the relation of recrossing effects (see below) to off-diagonal elements of the quantal width matrix [42].

Examination of nine published works from which q_α can be calculated showed that q_α was less than or equal to unity in eight [23,25,27,35,43-46] of them. The ninth reference [47] was concerned with shape resonances in the $\text{H}_2 X^1\Sigma_g^+$ system. In that paper, resonances were located (that is, ε_α and Γ_α were determined) by directly searching for the complex energy that gave rise to a pole in the scattering matrix. Then by solving the Schrödinger equation directly at complex energies z near z_α to determine $S_{n'n}(z)$, the partial widths were determined by numerically evaluating the contour integral around z_α

$$(1.18) \quad \oint S_{n'n}(z)dz = 2\pi\gamma_{\alpha n'}\gamma_{\alpha n}$$

This method of computing partial widths makes no assumptions about the background $S_{n'n}^b(E)$. For five of the twenty-two resonances characterized in Table 2 of Ref. 47, q_α differed from unity by more than 5%; the values of q_α in these cases were 0.85, 0.89, 1.06, 1.08 and 1.17. Thus this study gives examples where q_α exceeded unity. A mathematical analysis of the systematics of q_α and its dependence on the parameters of the scattering problem would be very useful.

2. Transition state resonances in reactive scattering. An important question posed by chemical dynamicists is whether the rates of chemical reactions are controlled by quantized dynamical bottlenecks. In other words, are there quantized structures in phase space that gate the flux of probability density from reactants to products, and, if so, is the gated flux quantized? The idea of a dynamical bottleneck is the central tenet in transition state theory [48-51], which postulates the existence of a structure in phase space - the "transition state" or "activated complex" - which controls chemical reactivity. In this section, we give an introduction to transition state theory and then summarize direct evidence which has been accumulated in accurate quantum dynamics calculations for a quan-

tized spectrum of the transition state. We then discuss the implications of the identification of transition states as resonances.

2.1. Transition state theory. We focus on the bimolecular reaction between A and BC, representing the transition state as ABC^\ddagger



The transition state is constrained to a hypersurface in phase space dividing the reactants from products [49-51]. This dividing surface has one less degree of freedom than the phase space itself; the missing degree of freedom, which is orthogonal to the dividing surface, is called the reaction coordinate and denoted s . The temperature dependent rate constant $k(T)$ that appears in the rate expression

$$(2.1) \quad -\frac{dC_A}{dt} = k(T)C_A C_{BC}$$

(where t denotes time) can be written, with the assumption that once the system gets to the transition state it inevitably proceeds to products, as

$$(2.2) \quad k(T) \cong \nu C_\ddagger^{\text{eq}}$$

where ν is the unimolecular rate constant for decay in the product direction of the transition state which has an equilibrium concentration C_\ddagger^{eq} . If we assume that $k(T)$ can be equated to the local-equilibrium phase-space flux in the product direction through the transition state hypersurface, then, in a classical world, one obtains [51]

$$(2.3) \quad k(T) \cong \frac{k_B T}{h} K_{\text{classical}}^\ddagger$$

where k_B is Boltzmann's constant and $K_{\text{classical}}^\ddagger$ is a kind of equilibrium constant which relates the product $C_A C_{BC}$ reactant concentrations to C_\ddagger^{eq} with the reaction coordinate removed in defining the hypersurface to which C_\ddagger^{eq} refers. $K_{\text{classical}}^\ddagger$ is computed via an integral over the phase space of the hypersurface [51]. In the quantal world, in which there would not be a *continuum* of transition state structures along the dividing surface but rather a *discrete set* of states on the hypersurface, eqn (2.3) becomes

$$(2.4) \quad k(T) \cong \frac{k_B T}{h} K_{\text{quantal}}^\ddagger$$

where $K_{\text{quantal}}^\ddagger$ is computed from the quantized partition functions (sums over discrete sets of levels) of A, BC, and the transition state hypersurface (again with motion along the reaction coordinate removed). Eqn (2.4), in effect, postulates the existence of a set of discrete levels associated with

the transition state hypersurface orthogonal to the reaction coordinate. We will seek evidence in the accurate quantal calculations for these levels of the transition state; in other words, we seek to perform transition state spectroscopy, a term used in a series of papers by Polanyi and coworkers [52].

If the analysis that led to eqn (2.4) is repeated for a microcanonical ensemble (a system at fixed total energy rather than fixed temperature), the transition state theory rate constant $k^{TS}(E)$ at a given energy E can be written as [53-58]

$$(2.5) \quad k^{TS}(E) = \frac{N^{TS}(E)}{h\rho^R(E)}$$

where $N^{TS}(E)$ is the number of energy levels of the activated complex with energies less than or equal to E , and $\rho^R(E)$ is the reactants' density of states per unit energy per unit volume. The quantity $N^{TS}(E)$ increases, obviously, by one at each of the energy levels of the transition state.

An exact quantum mechanical expression for the microcanonical rate constant $k(E)$ can be written as [19,54]

$$(2.6) \quad k(E) = \frac{N(E)}{h\rho^R(E)}$$

where $N(E)$, which is called the cumulative reaction probability (CRP) [59], is a double sum over all the state-to-state reaction probabilities at an energy E :

$$(2.7) \quad N(E) = \sum_n \sum_{n'} P_{n \rightarrow n'}(E)$$

For an atom-diatom reaction, $n(n')$ is an index representing the total angular momentum J , its component M_J on an arbitrary space-fixed axis, and a set of initial (final) vibrational quantum number $v(v')$, rotational quantum number $j(j')$ and orbital angular momentum quantum number $l(l')$. The CRP can be written in terms of the scattering matrix elements $S_{n'n}$ as [60]

$$(2.8) \quad N(E) = \sum_n \sum_{n'} |S_{n'n}|^2$$

Comparison of eqns (2.5) and (2.6) suggests, if the quantization of the transition state is taken literally, that the quantal CRP should increase in steps of one at each of the energy levels of the transition state. However, this analysis has neglected quantum mechanical tunneling at energies below the transition state energy level as well as nonclassical reflection above the energy level. In addition, it has been assumed up to this point that the transition state is a perfect dynamical bottleneck, i.e. systems crossing the activated complex hypersurface go right from reactants to products without

recrossing the dividing surface [51,57,61-64]. Generalizations of transition state theory have been proposed to account for these effects [54,58,59,65]. For example, one way to account for the effects of recrossing, tunneling and reflection, which we will use extensively in the next section, is to make the replacement

$$(2.9) \quad N^{TS}(E) \rightarrow \sum_{\tau} \kappa_{\tau} P_{\tau}(E)$$

in eqn (2.5), where τ is the index of a level of the transition state, κ_{τ} is a transmission coefficient accounting for recrossing (more precisely, for the quantal analog of classical trajectories that reach the transition state hypersurface and then recross it - either before proceeding to products or without ever proceeding to products [51,57,58]), and P_{τ} is a transmission probability accounting for tunneling and reflection. Invoking substitution (2.9), we see that the numerator of eqn (2.5) still contains a sum over energy levels of the transition state but instead of increasing abruptly by a step of unity at each new level of the activated complex, it will now increase more gradually, by an amount given by $\kappa_{\tau} P_{\tau}(E)$. If we denote the transition state energy level as E_{τ} , then for an ideal dynamical bottleneck, κ_{τ} is unity, and $P_{\tau}(E)$ is expected to rise smoothly from zero at energies E well below E_{τ} to unity at energies well above E_{τ} . Thus transition state theory incorporating (2.9) predicts that the quantal CRP will increase in smooth steps of height κ_{τ} at each new energy level of the transition state. We have found clear evidence of such behavior in accurate quantal scattering calculations, as described below.

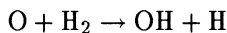
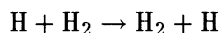
2.2. Characterization of quantized transition states in chemical reactions. Most approximate theoretical treatments of chemical reaction rates involve the concept of a transition state, i.e. a dynamical bottleneck. But, up until the time we began our studies, the spectrum of this mathematical construct had never been directly observed, and one may have questioned its physical significance. Thus we have sought to address the question of whether one can observe the quantized nature of dynamical bottlenecks in chemical reaction dynamics. To seek an answer, we have performed accurate three-dimensional quantal scattering calculations for three-body systems interacting according to realistic potential energy surfaces, and, via analysis of the cumulative reaction probability, we have looked for evidence of quantized dynamical bottlenecks.

We can study the reaction dynamics for each value of the total angular momentum J independently since it is conserved during the collision. Its component M_J is also conserved and since results are independent of M_J , we always set it to zero and forget about it. The J -specific contribution to the CRP is denoted $N^J(E)$ and it is computed from the sum over J -specific channel-to-channel transition probabilities $P_{n \rightarrow n'}^J(E)$ in a manner analogous to eqn (2.7). The dynamical structure in the reaction rate constant is most clearly brought out by computing the energy derivative of

the cumulative reaction probability, which is called the density of reactive states. The J -specific density of reactive states is defined as

$$(2.10) \quad \rho^J(E) = \frac{dN^J(E)}{dE}$$

We have looked for, and found, evidence of quantized transition states in a number of three-dimensional chemical reactions, including $\text{H}+\text{H}_2$ [19-21], $\text{O}+\text{H}_2$ [21,66-68], $\text{D}+\text{H}_2$ [69,70], $\text{F}+\text{H}_2$ [70,71], $\text{Cl}+\text{H}_2$ [70,72], $\text{Cl}+\text{HCl}$ [73], $\text{I}+\text{HI}$ [73], and $\text{I}+\text{DI}$ [73]. In addition, the conclusions reached in these studies have been supported by a number of accurate calculations by other research groups on other atom-diatom systems including $\text{He}+\text{H}_2^+$ [74], $\text{Ne}+\text{H}_2^+$ [75], $\text{H}+\text{O}_2$ [76], and $\text{O}+\text{HCl}$ [77]. Here we will focus on just two of the systems we have studied:



The first is the simplest and theoretically most-studied atom-diatom neutral reaction [78] and the first system for which we found evidence of global control of reactivity by a spectrum of quantized transition state levels. The second is also of interest because it is asymmetric (reactants and products are different chemical species), and this introduces the possibility of multiple bottleneck regions with transition states having different sets of energy levels on the reactant ($\text{O}+\text{H}_2$) side and on the product ($\text{OH}+\text{H}$) side.

For the above two reactions, we made the Born-Oppenheimer separation of electronic and nuclear motions [79], and we assume that the scattering event can be treated as the motion of three bodies (in full three-dimensional space) interacting through a single effective potential energy surface. The quantal results to be presented result from treating the two hydrogen atoms in the reactant H_2 molecule as distinguishable and giving results for one of the two possible sets of products, for example, $\text{A} + \text{H}_a\text{H}_b \rightarrow \text{AH}_a + \text{H}_b$. Therefore, the factor of 2 for the products $\text{AH}_a + \text{H}_b$ and $\text{AH}_b + \text{H}_a$ is not included in the CRP nor the density of reactive states. The computational methods used to calculate accurate quantal CRPs and densities are briefly summarized in Appendix I.

2.2.1. $\text{H} + \text{H}_2$. The $J = 0$ cumulative reaction probability $N^0(E)$ was computed [19,20] from converged scattering matrix elements via eqn (2.8). The calculation employed the accurate double many-body expansion (DMBE) potential energy surface [80] for H_3 . It was found that $N^0(E)$ is characterized by a series of smooth steps as predicted by transition state theory and discussed at the end of Section 2.1. Differentiation of a cubic spline fit to $N^0(E)$ yielded $\rho^0(E)$, the $J = 0$ density of reactive states; steps in N^0 were converted to peaks in ρ^0 . The CRP reaches a value of 8.9 at 1.6 eV (we use energy units of eV; 1 eV/molecule = 96.48 kJ/mol). Thus if

all transition states are perfect dynamical bottlenecks ($\kappa_\tau = 1$), transition state theory predicts nine energy levels of the quantized transition state at energies below 1.6 eV. From the analysis described in the following paragraphs, it was concluded that in fact ten energy levels contribute to the CRP and density of reactive states.

If an explicit functional form were available for the transmission probability $P_\tau(E)$, it would be desirable, based on eqn (2.9), to fit the accurate quantal CRP to

$$(2.11) \quad N(E) = \sum_{\tau} \kappa_{\tau} P_{\tau}(E)$$

The fit would reflect the degree to which the quantal dynamics follow the predictions of transition state theory and also would allow us to extract parameters (such as κ_τ) characteristic of each transition state level τ .

To obtain a simple form for $P_\tau(E)$, we assume that there exists an effective potential energy barrier $V_\tau(s)$ for passage through the transition state region in level τ . We furthermore assume that the potential barrier is parabolic, having the form

$$(2.12) \quad V_\tau(s) = E_\tau + \frac{1}{2} k_\tau s^2$$

where E_τ is the energy of the barrier maximum and k_τ is a negative force constant. Recall that the parameter E_τ also represents the energy of transition state level τ . Therefore, within this simple model, each level of the transition state is associated with a maximum in an effective potential barrier. In the case of a parabolic barrier, the quantum mechanical transmission probability P_τ is [81]

$$(2.13) \quad P_\tau(E) = \frac{1}{1 + \exp[(E_\tau - E)/W_\tau]}$$

where W_τ is a width parameter given by

$$(2.14) \quad W_\tau = \frac{\hbar|\omega_\tau|}{2\pi}$$

with ω_τ the imaginary frequency of the barrier

$$(2.15) \quad \omega_\tau = \sqrt{k_\tau/\mu}$$

and μ the reduced mass. As anticipated, $P_\tau(E)$ rises smoothly from zero to one, accounting for tunneling and nonclassical reflection.

Since dynamical structure is brought out more clearly in the density of reactive states, it is advantageous to fit the accurate density as

$$(2.16) \quad \rho(E) = \sum_{\tau} \left[\kappa_{\tau} \frac{dP_{\tau}(E)}{dE} \right]$$

Taking the energy derivative of $P_\tau(E)$ in eqn (2.13), we arrive at an expression useful for fitting the density of reactive states:

$$(2.17) \quad \rho(E) = \sum_{\tau} \kappa_{\tau} \rho_{\tau}(E)$$

where

$$(2.18) \quad \rho_{\tau}(E) = \frac{\exp[(E_{\tau} - E)/W_{\tau}]}{W_{\tau}(1 + \exp[(E_{\tau} - E)/W_{\tau}])^2}$$

The function $\rho_{\tau}(E)$ is a symmetric bell-shaped curve centered at E_{τ} ; the wider the effective potential barrier $V_{\tau}(s)$ (the smaller the k_{τ}), the smaller the width parameter W_{τ} and the narrower the function $\rho_{\tau}(E)$. The accurate quantum scattering calculations [19] showed that the transition state theory prediction that the density of reactive states will be a sum of bell-shaped curves, each centered at some energy E_{τ} , appears to hold true for the density $\rho^0(E)$ for H+H₂. The strategy should now be clear; by fitting the accurate quantal density to a sum of terms $\kappa_{\tau}\rho_{\tau}(E)$, as given in eqn (2.17), we can determine the fitting parameters κ_{τ} , E_{τ} and W_{τ} for each transition state level τ .

A fit to $\rho^0(E)$ for H+H₂ using 10 terms in eqn (2.17) yields a curve which is nearly indistinguishable from the quantal result [19,21]. Integration of the fit to ρ^0 yields the fitted CRP curve which is indistinguishable from $N^0(E)$ to plotting accuracy.

The excellent agreement between the quantal and fitted densities of reactive states shows convincingly that the chemical reactivity is globally controlled by quantized transition states. All of the reactive flux up to an energy of 1.6 eV can be associated with energy levels of the transition state; there is no discernible background contribution. In addition, we can assign the quantized transition state structure to specific vibrational-rotational levels of the transition state, as discussed in the following paragraphs.

A quantized transition state of H₃ is a short-lived state (a resonance; see Section 2.3) with a set of linear-triatomic quantum numbers [82] $[v_1 v_2^K]$, where v_1 and v_2 are the stretch and bend quantum numbers, respectively, for modes orthogonal to the reaction coordinate and K is the vibrational angular momentum, the projection of J on the molecular axis. Whereas a stable triatomic molecule like CO₂ has a complete set of quantum numbers $(v_1 v_2^K v_3)$ with v_3 being the asymmetric stretch quantum number [82], the H₃ transition state appears to have one quantum number missing, corresponding to unbound motion along the reaction coordinate. The $[v_1 v_2^K]$ labelling therefore corresponds to the classical picture of the transition state being a hypersurface in phase space. We will see in Section 2.3 that in the quantum mechanical treatment of the transition state as a resonance, the 'missing' quantum number will reappear.

The lowest energy feature for H+ H₂ is readily assigned as $[00^0]$ since it is the overall reaction threshold and therefore corresponds to the lowest

energy level of the transition state. The remainder of the assignments were made primarily by comparing the fitted E_τ values with features in semiclassical vibrationally adiabatic potential energy curves. The latter are defined by [65,83-87]

$$(2.19) \quad V_a(v_1, v_2, K, J, s) = V_{\text{MEP}}(s) + \varepsilon_{\text{int}}(v_1, v_2, K, J, s)$$

where s is the distance along the reaction path, V_{MEP} is the Born-Oppenheimer potential energy along the reaction path, and ε_{int} is the vibrational-rotational energy of the stretch, bend and rotational motions excluding motion along the reaction coordinate. The stretching motion (with quantum number v_1) of the H_3 transition state correlates adiabatically with vibrational motion (with quantum number v) in the reactant H_2 [88]. The energies of the maxima in the vibrationally adiabatic curves are in good agreement with the fitted values of E_τ and allowed us to make the assignments. Furthermore, this good agreement strongly suggests that the reactive flux is "focused" [89] through dynamical bottlenecks that are locally vibrationally adiabatic. However, the quantal calculations [19,20] demonstrate that the overall chemical reaction is not *globally* adiabatic; e.g. many of the $P_{n \rightarrow n'}$ with $v \neq v'$ are significant in magnitude ($> 10^{-3}$). Thus reactive flux which is channelled through a particular $[v_1 v_2^K]$ level of the transition state need not originate from only those reactant states with $v = v_1$ but may originate from a wide set of reactant states; this point will be addressed in more detail in Section 2.3 below. One way to understand why the dynamics, although not globally adiabatic, is *locally* adiabatic at the transition state is to note that motion along the reaction coordinate is classically stopped at a barrier maximum. Thus the simplest criterion for vibrational adiabaticity, that vibrational motions normal to the reaction coordinate be fast compared to motion along the reaction coordinate, is satisfied locally.

With the assignments $[v_1 v_2^K]$ made, we can note several important trends in the fitted values of the transmission coefficient. We found that six of the first nine levels of the transition state are ideal dynamical bottlenecks with $\kappa_\tau \cong 1.0$. Deviations from unity are found for only a few of the levels, with the most significant breakdown of transition state theory being associated with a highly bend-excited level. We can also understand trends in the widths (W_τ values) of the quantized transition state features in terms of the widths of the vibrationally adiabatic potential curves; these kinds of trends have been discussed in detail in Refs. [11,12,20,21].

2.2.2. O + H₂. The accurate density of reactive states for $\text{O}(^3\text{P}) + \text{H}_2$, $J = 0$ was studied [66-68] using the Johnson-Winter-Schatz potential energy surface [90,91]. At energies below 1.3 eV, the density ρ^0 for this reaction looks strikingly similar to that of $\text{H} + \text{H}_2$ [19,21]. In fact, it turns out that the first six assignments $[v_1 v_2^K]$ are identical for the two systems [68]. Above 1.3 eV, however, the $\text{O} + \text{H}_2$ density exhibits more peaks due

to a greater number of levels of the quantized transition state.

The density $\rho^0(E)$ for O+H₂ was fit using 17 terms in eqn (2.17) and the quantal and fitted densities are indistinguishable to plotting accuracy [68]. Many of the quantized transition states are nearly ideal dynamical bottlenecks; i.e. many κ_τ for values are close to unity. The excellent fit to $\rho^0(E)$ for O+H₂ demonstrates that quantized transition states globally control the reaction dynamics, as they did for H + H₂.

To assist in making assignments of the transition states, vibrationally adiabatic potential energy curves were computed using the same methods as for H + H₂ [68]. Unlike the curves for H+H₂, many of those for the O + H₂ reaction show two distinct transition states, one on the reactant side and one on the product side, each with its own set of energy levels. In such cases, it is interesting to see if bottlenecks in both regions influence the chemical reactivity. Each of the computed vibrationally adiabatic potential curves with $v_1 \geq 1$ exhibited several local maxima. Only the first and last local maxima of each curve can be associated with dynamical bottlenecks because only in the vicinity of these two maxima is the dynamics predicted, semiclassically, to be vibrationally adiabatic. If the chemical reaction were vibrationally adiabatic (i.e. $P_{n \rightarrow n'} = 0$ for all $v \neq v'$), only the higher of the two maxima, which appears at a reaction coordinate nearer to the reactants, would have an impact on the reactivity. We call these reactant-like bottlenecks *variational* transition states and designate them in the usual way, $[v_1 v_2^K]$. However, since the O + H₂ reaction has many nonnegligible $v \neq v'$ reaction probabilities, we know that the reaction is not globally vibrationally adiabatic and, therefore, it is possible that product-like dynamical bottlenecks influence the reactivity. We call these latter bottlenecks *supernumerary* transition states and denote them as $S[v_1 v_2^K]$.

The correspondence between the fitted values of E_τ and the global maxima in the 00⁰ and 10⁰ vibrationally adiabatic potential curves allowed [68] us to unambiguously assign the first and third features in the density curve to the [00⁰] and [10⁰] variational transition states. In addition, ρ^0 exhibits peaks at the energies of both the reactant-like and product-like maxima in the $v_1 = 2, v_2 = 0$ and $v_1 = 3, v_2 = 0$ vibrationally adiabatic curves. This allowed [68] us to identify two more variational transition states, [20⁰] and [30⁰], as well as two supernumerary transition states $S[20^0]$ and $S[30^0]$.

The remaining assignments were made largely [68,70] on the basis of analysis of channel-selected transition probabilities $P_n^J(E)$ defined as

$$(2.20) \quad P_n^J(E) = \sum_{n'} P_{n \rightarrow n'}^J(E)$$

The quantity defined above gives the total reactive transition probability coming out from a specified initial (reactant) channel n by summing over all possible *final* channels n' . (By then summing $P_n^J(E)$ over all *initial* channels n , we retrieve the J -specific cumulative reaction probability.) We can then

define the corresponding density of channel-selected reaction probability $\rho_n^J(E)$

$$(2.21) \quad \rho_n^J(E) = \frac{dP_n^J(E)}{dE}$$

Similarly, we can make the analysis in terms of product channels n' :

$$(2.22) \quad P_{\rightarrow n'}^J(E) = \sum_n P_{n \rightarrow n'}^J(E)$$

$$(2.23) \quad \rho_{\rightarrow n'}^J(E) = \frac{dP_{\rightarrow n'}^J(E)}{dE}$$

The quantities defined in eqns (2.22) and (2.23) provide useful information on the total reactive transition probability going into a specified final (product) channel n' .

The channel-selected densities (2.21) and (2.23) provide valuable information on how flux through a given level of the transition state couples with particular reactant and product states. In particular, when both supernumerary and variational transition states influence chemical reactivity, the former are primarily observed in $\rho_{\rightarrow n'}^J$ and the latter primarily in ρ_n^J . We can most easily understand this by recognizing that, from the principle of time reversal invariance, $P_{n \rightarrow n'}^J$ describes both forward ($n \rightarrow n'$) and reverse ($n' \rightarrow n$) reactions. Therefore, whereas ρ_n^J describes reaction *out* of channel n for the *forward* reaction, $\rho_{\rightarrow n'}^J$ describes reaction *out* of channel n' for the *reverse* reaction. Thus, the quantity ρ_n^J will tend to be influenced by reactant-like (variational) transition states and $\rho_{\rightarrow n'}^J$ by product-like (supernumerary) transition states. By calculating channel-selected densities for O+H₂ and identifying maxima in the density curves as features due to variational and/or supernumerary transition states, we were able to assign most of the spectrum [68,70].

2.3. Interpretation of transition states as resonances. We have found strong evidence in quantal calculations, as discussed above, for the control of chemical reactivity by quantized transition states which can be thought of as being associated with the potential maxima of vibrationally adiabatic potential curves. In fits to the quantal density of reactive states, we have taken the energy levels of the transition states to be the potential energy maxima of effective parabolic barriers.

The parabolic barrier of eqn (2.12) has poles of the scattering matrix which are found at [10,21,92,93]

$$(2.24) \quad E_\nu = E_\tau - i\hbar|\omega_\tau|(v + \frac{1}{2})$$

where $v = 0, 1, 2, \dots$ labels the pole. Thus, there is a sequence, an infinite one in fact, of overlapping poles of the S matrix whose complex resonance

energies all have a real part E_τ . The widths increase along the sequence as $2v+1$. This analysis and other studies of one-dimensional potential barriers in Section 3 show unambiguously that passage over a potential barrier is associated with poles in S , from which we can conclude that quantized transition states are reactive scattering resonances, which we refer to as barrier resonances. Note that we can associate the quantum number v which labels the poles for a given parabolic barrier with the 'missing' quantum number v_3 of the transition state corresponding to the 'missing' degree of freedom. (We point out here that a series of poles labelled by v is not unique to a parabolic barrier; for approximately parabolic barriers, as well, the labelling of members of a sequence of poles by a quantum number v emerges, as discussed in Section 3.)

However, there is an apparent paradox presented by the above discussion. Analyses of the poles of the scattering matrix show that even for a simple barrier (parabolic or approximately parabolic), there is more than one pole [10-12,92-94]. On the other hand, work on three-dimensional quantal dynamics such as that described in Section 2.2 shows that the cumulative reaction probability and density of reactive states are influenced by a small number of quantized transition states. In particular, the density can be fit extremely well using a model of scattering in which each effective parabolic potential barrier V_τ is associated with *one* level of the transition state at a real energy E_τ . This apparent paradox has more than one possible resolution. The simplest is to assume that only the poles close to the real axis have an appreciable effect on the dynamics. Then, since poles with $v \geq 1$ are three more times farther from the real axis than the corresponding poles with $v = 0$, one could consider only the $v = 0$ poles. Unfortunately, we know that the situation is not really quite so simple. Although the $v = 0$ poles provide a good quantitative account of the transition state energies and lifetimes [21], they do not account quantitatively for $P_\tau(E)$ [92]. Nevertheless when combined with a short-time correction, the sum over the $v = 0, 1, 2, \dots$ states is rapidly convergent, giving reasonable results with 2 states and quite good results with 4 – 8 states [92]. It is encouraging though that the initial state count in $N^{TS}(E)$ requires only the $v = 0$ states. One could imagine cases where the progressions in v are not readily assignable due to mixed character in the Siegert eigenfunctions [16] associated with the poles. Then a state might show mixed character such as 50% of $v = 0$ in the reaction coordinate with some set of quantum numbers τ for other degrees of freedom and 50% of some other combination, $(v'\tau')$, with $v' \neq 0$. Then it would be unclear whether to count this state in $N^{TS}(E)$. Such a situation would seem to indicate that one cannot identify a separable reaction coordinate, which is a necessity for applying transition state theory. Mathematical analysis clarifying the effect of various barrier poles on the rate constant would be very useful.

The $v = 0$ pole of the parabolic barrier has a width given by $\hbar|\omega_\tau|$, where we have used the general definition of the complex resonance energy

given in eqn (1.1). We equate this resonance width with that of level τ of the quantized transition state characterized in the fits to $\rho(E)$. The resonance width is related to the collision lifetime $\Delta\tau$ by [95]

$$(2.25) \quad \Delta\tau = 2\hbar/\Gamma$$

and upon substitution of Γ by $\hbar|\omega_\tau|$ and using eqn (2.14), one obtains

$$(2.26) \quad \Delta\tau = \frac{2}{|\omega_\tau|} = \frac{\hbar}{\pi W_\tau}$$

From the W_τ values obtained in the fit to the density of reactive states for $\text{H} + \text{H}_2$ and given in Ref. 20, we calculated collision lifetimes via eqn (2.26). These lifetimes, labelled transition state resonance theory, are shown in Table 1 for the case of $J = 0$ discussed above and in addition for the case of $J = 1$ described elsewhere [20]. The transition state lifetimes range from 5 to 30 femtoseconds. They are compared in Table 1 to collision lifetimes computed [8] from accurate quantal scattering matrix elements without transition state theory or resonance theory. Since the W_τ values are obtained from fits to the energy dependence of reaction probabilities which do not depend on the phases of S matrix elements while the direct calculation [8,32,33] of collision lifetimes depends explicitly on phase information, there is no reason a priori why the two columns in Table 1 need agree. The fact that they do provides further evidence for the usefulness of treating transition states by resonance theory.

Furthermore, we can proceed to obtain spectroscopic constants for the quantized transition states, which are associated with poles of the scattering matrix at complex resonance energies $E_\tau - i\pi W_\tau$ (see above). By analogy to the procedure for getting spectroscopic constants for bound states [82], constants for the transition states can be obtained by fitting the resonance energies to the form

$$(2.27) \quad \begin{aligned} E_\tau(v_1, v_2) - i\pi W_\tau(v_1, v_2) &= E_0 + hc\omega_1(v_1 + 0.5) + hc\omega_2(v_2 + 1) \\ &+ x_{11}(v_1 + 0.5)^2 + x_{22}(v_2 + 1)^2 \\ &+ x_{12}(v_1 + 0.5)(v_2 + 1) + BJ(J + 1) \end{aligned}$$

where E_0 is a constant and $\omega_1, \omega_2, x_{11}, x_{12}, x_{22}$, and B are the spectroscopic fitting parameters, and c is the speed of light in a vacuum. Since we fit in eqn (2.27) both the energies E_τ and the widths W_τ of the quantized transition states, all of the fitting parameters, including E_0 , are complex.

As a specific example of a spectroscopic fit we consider the $\text{O} + \text{H}_2$ quantized transition states discussed above. A least squares fit of the first six levels resulted in the following values (in wavenumber units of cm^{-1}) of the complex spectroscopic constants for the variational transition states:

$$\begin{aligned} E_0 &= 3786 - 597i & \omega_1 &= 2241 + 507i & \omega_2 &= 737 - 307i \\ x_{12} &= -45 - 89i & x_{22} &= -2 + 43i \end{aligned}$$

TABLE 1
Lifetimes (fs) for H + H₂ quantized transition states.

<i>J</i>	<i>E_τ</i> (eV)	transition state	
		resonance theory ^a	accurate ^b
0	0.65	10	11
	0.87	7	10
	0.98	28	28
	1.09	6	5
	1.19	10	8
1	0.65	10	11
	0.76	8	9
	0.88	7	10
	0.98	27	28
	0.99	6	8
	1.09	16	29
	1.10	10	5
	1.19	10	8
	1.21	7	6

^aFrom eqn (2.26) and *W_τ* values given in Ref. 20

^bFrom Ref. 8

We constrained the values of *x*₁₁ and *B* to zero because none of the first six levels involve *v*₁ > 1 or *J* > 0.

The interpretation of transition states as reactive scattering resonances also enables us, through an analysis of channel-selected densities, to obtain information concerning the partial widths of these barrier resonances [20,21]. We considered channel-selected densities, and found that the major peaks in ρ_n^0 and ρ_{-n}^0 , occur at or very near the values of *E_τ* determined earlier from the fit to the overall density of reactive states. We thus see that quantized levels of the transition state control state-selected as well as total chemical reactivity. For example, for H + H₂ with *J* = 0, reactive flux emanating from the *v* = 0, *j* = 4 channel passes predominantly through only the [02⁰] and [20⁰] levels of the transition state at their threshold energies. We find in general [20,21] that the asymptotic channels couple primarily to only a few transition state levels and, in particular, mainly to one or two consecutive bending (*v*₂) levels with stretch quantum number *v*₁ equal to channel vibrational quantum number *v*. Therefore, there is a large propensity for stretch adiabaticity (*v* = *v*₁) in the half collisions that take the system from reactants to the transition state.

To characterize quantitatively which asymptotic channels couple to which quantized levels of the transition state, we [20,21] fit $\rho_n^0(E)$ with a sum of lineshapes for scattering by parabolic potential energy barriers, just

as we did for the total density in eqn (2.17):

$$(2.28) \quad \rho_n(E) = \sum_{\tau} \kappa_{\tau n} \rho_{\tau}(E)$$

where $\rho_{\tau}(E)$ is given in eqn (2.18) with the values of E_{τ} and W_{τ} fixed at those values determined in the fit to the total density. The parameter $\kappa_{\tau n}$, which was determined using linear least squares, is a measure of the amount of reactive flux passing through transition state level τ at energy E_{τ} that originated from a specific state n . When all the values of $\kappa_{\tau n}$ for a particular level τ are summed, we retrieve the value of the transmission coefficient κ_{τ} of eqn (2.17). Since the ratio $\kappa_{\tau n}/\kappa_{\tau}$ represents how much of the total reactive flux passing through level τ of the transition state at energy E_{τ} originated from channel n , we can identify the partial width for entering the level τ at energy E_{τ} from incident channel n as (within our model of scattering off parabolic barriers)

$$(2.29) \quad \Gamma_{\tau n} = \frac{\kappa_{\tau n}}{\kappa_{\tau}} \Gamma_{\tau}$$

with

$$(2.30) \quad \Gamma_{\tau} = 2\pi W_{\tau}$$

Although eqn (2.29) would require, by definition, that the INR formula, (1.6), be strictly followed, which of course we don't expect to be the case for broad barrier resonances, eqn (2.29) is nonetheless useful because it provides a type of detailed picture of the reactive event that is available in no other way that does not involve analyzing wave functions.

By calculating the ratio of $\kappa_{\tau n}$ to κ_{τ} for each channel n and each level τ , we have determined which channels make significant partial width contributions to each level of the transition state [20,21]. Some results are presented in Table 2 for the low bend (v_2) states with $v_1 = 0, 1, 2$. M_{ad} and M_{nonad} are the number of initial channels which make stretch adiabatic ($v = v_1$) and stretch nonadiabatic ($v \neq v_1$) contributions, respectively, of at least 5% to the total reactive flux (i.e. $\kappa_{\tau n}/\kappa_{\tau} \geq 0.05$). The table's entries are percent contributions for those channels having a specified value of $|j - v_2|, v = v_1$; for example, 27% of the reactive flux passing through [00⁰] at its E_{τ} value originates from the channel with $|j - v_2| = 2$, that is, channel ($v = 0, j = 2$). When several initial channels with the same value of $|j - v_2|$ contribute, the number of channels is indicated in brackets, and the sum of their percent contributions is shown. We see from the table that the largest partial widths tend to be for those channels with $v = v_1$ and $|j - v_2| \leq 3$. Partial widths for channels with $v \neq v_1$ tend to become more important for high v_1 .

If one pursues the identification of dynamical bottlenecks with resonances, the description of chemical reactivity ultimately becomes a quest

TABLE 2

State-selected contributions to the total reactive flux passing through thresholds for $H + H_2$ with $J = 0$ and 1.

threshold ^a	M_{ad}	M_{nonad}	$ j - v_2 $ for $v = v_1$					
			0	1	2	3	4	> 4
[00 ⁰]	4	0	22	41	27	9	0	0
[01 ¹]	4	0	15	35	32	15	0	0
[02 ⁰]	5	0	0	21	42 [2] ^b	23	6	0
[10 ⁰]	3	0	33	51	20	0	0	0
[11 ¹]	3	0	24	45	26	0	0	0
[12 ⁰]	5	1	7	34	37 [2]	10	0	0
[20 ⁰]	2	6	13	17	0	0	0	0
[21 ¹]	3	2	28	41	13	0	0	0
[22 ⁰]	4	3	9	31	24 [2]	0	0	0

^a Results for even v_2 transition states from $J = 0$ quantal calculations. Results for $v_2 = 1$ transition states from $JP = 1+$ quantal calculations (P being the parity).

^b For example, two initial channels with $v = v_1 = 0$, $|j - v_2| = |j - 2| = 2$ have contributions to the total reactive flux passing through [02⁰] at its threshold energy of greater than 5% and the sum of their percent contributions is 42.

to find, label, and characterize the set of resonances resulting from a many-body potential energy function. Resonances often provide simple explanations of complex observable phenomena, so we are motivated to develop a better understanding of resonances in many-body reactive systems.

The success in using a simplistic model of transmission through effective potential energy barriers to fit the total and channel-selected densities of reactive states and obtain resonance parameters for quantized transition states (as well as the good agreement between transition state energy levels and the maxima of semiclassical vibrationally adiabatic curves) in three-body, multichannel problems strongly suggests that detailed studies of scattering by one-dimensional potential barriers can provide further insight on barrier resonances. We have already seen how the analysis of the scattering matrix for the one-dimensional parabolic barrier proved useful in the interpretation of transition states as resonances. In the following section, we present results from other one-dimensional studies on both symmetric and asymmetric potential energy barriers.

3. Barrier resonances in one-dimensional studies.

3.1. Barrier passage and poles of the S matrix. The most widely used model for a chemical reaction is passage over a potential energy barrier. The potential maximum is associated with the reaction threshold for

which we can provide insight via quantum mechanical studies of scattering by one-dimensional potential energy functions.

In two published studies [11,12] we have considered scattering in one dimension x off a potential barrier $V(x)$ with boundary conditions in the two limits $x \rightarrow \pm\infty$. In this two-channel (left-right) scattering problem, we let channel 1 denote the asymptotic region on the left ($x \rightarrow -\infty$) and channel 2 denote that on the right ($x \rightarrow +\infty$). We solve the Schrödinger equation

$$(3.1) \quad \frac{d^2\psi}{dx^2} + \frac{2\mu}{\hbar^2}[E - V(x)]\psi(x) = 0$$

where $\psi(x)$ is the wavefunction and determine the unitary scattering matrix \mathbf{S} . From scattering matrix elements computed at real energies E , we can calculate transmission and reflection coefficients [96]

$$(3.2) \quad P_{ij} = |S_{ji}|^2$$

as well as channel-to-channel delay times Δt_{ij} given by eqn (1.14). Furthermore, by directly solving the Schrödinger equation at complex energies [11,12,44,47], we search for poles of the S matrix; this allows us to find and characterize both narrow and broad resonances. The computational methods we used to solve eqn (3.1) are briefly described in Appendix II.

3.1.1. Symmetric potential functions. In the first study [11], we considered symmetric potential barrier functions of the form

$$(3.3) \quad V(x) = V_0 \left(\frac{e^{\beta x}}{(1 + e^{\beta x})^2} - \frac{\alpha}{2} \frac{e^{5\beta x}}{(1 + e^{5\beta x})^2} \right)$$

and the potential parameters were chosen to roughly resemble a one-dimensional model [97] of the $\text{H} + \text{H}_2$ reaction, in particular $\mu = \frac{2}{3}m_{\text{H}} = 1224.5m_e$, $V_0 = 2.177$ eV, and $\beta = 1a_0^{-1}$. When $\alpha = 0$, the potential is a simple Eckart barrier [98] and when this dimensionless parameter is greater than zero, the potential has twin maxima on either side of the $x = 0$ local minimum.

Reaction probabilities P_{12} , reactive delay times Δt_{12} and the locations of poles of the scattering matrix \mathbf{S} were calculated for many values of α . A curve connecting the pole locations maps out their ‘trajectory’ in the complex energy plane as a function of α .

The various cases have been discussed at length in Ref. 11; here, we simply highlight the main features. For the pure Eckart potential, which corresponds to $\alpha = 0$, there is no structure in $V(x)$ other than the barrier maximum. In the vicinity of the potential maximum there is a smooth rise in the reaction probability from zero to unity and a maximum in the delay time of 33 fs. The real part ε_α of the resonance energy is close to the energy of the barrier maximum V_{max} and clearly demonstrates that passage over a potential barrier is associated with a pole of the \mathbf{S} matrix.

For $\alpha = 0.17$ and 0.32 , the real parts of the resonance energies are slightly above V_{\max} . We also begin to see more structure for these cases in the reaction probability; P_{12} decreases slightly after its initial rise to unity and then returns to unity.

When $\alpha = 0.49$ there are two poles, one with ε_α below V_{\max} and one above V_{\max} . The dip in P_{12} after the threshold is more prominent and is beginning to be associated with a second feature in Δt_{12} . This shoulder in the delay time is clearly associated with the second very broad resonance coming from far off the real energy axis and 35 meV above V_{\max} . For the four cases $\alpha = 0 - 0.49$, see that as the width Γ_α of the resonance decreases, the peak in the delay time increases.

The barrier resonance for $\alpha = 0 - 0.32$ is in the process of becoming a subthreshold trapped-state resonance for $\alpha = 0.49$ as the parameter α is varied. When $\alpha = 0.68$, the process is complete; there is a narrow trapped-state resonance 37 meV below V_{\max} and a broad ($\Gamma_\alpha = 111$ meV) resonance 39 meV above V_{\max} associated with the rise in the reaction probability from 0.2 to 1.0.

As the well in the potential function $V(x)$ gets deeper for $\alpha = 0.68 - 1.60$, the resonance with the smaller value of ε_α moves lower and lower in energy relative to V_{\max} and is associated with an increasingly larger delay time Δt_{12} , consistent with its decreasing width [11]. It is obvious that what was once a barrier resonance is now clearly a trapped-state resonance, responsible for the sharp variation in the reaction probability from zero to unity and then almost back to zero. At the same time, the second very broad resonance first identified for $\alpha = 0.49$ is moving closer to the real energy axis and to the energy of the barrier maximum. For example, the broad resonance for $\alpha = 1.00$ has about the same width (and associated delay time) as the pole associated with the pure Eckart barrier. In addition there is an indication of a third resonance when $\alpha = 1.60$, as evidenced by a deep dip in P_{12} above V_{\max} and by the hint of another feature in Δt_{12} at about 75 meV above the potential maximum. The story told with $\alpha = 0 - 0.49$ clearly repeats itself for $\alpha = 0.68 - 1.60$ [11].

In summary, this study showed that by varying the parameters of the potential function to change it from having a single maximum to having two maxima with a dip between them, one pole of the scattering matrix is transformed continuously from a barrier resonance (describing the threshold of a simple potential barrier) to a trapped-state resonance (describing a state trapped in the well between barriers). In the meantime, a second resonance comes into the picture above V_{\max} and moves from a metastable state above threshold to a metastable state associated with the threshold, and it is in the process of turning into a second-trapped state when our picture stops. As α is further increased, the poles will move eventually onto the negative real energy axis and become bound states.

We discuss below the quantitative relation between the resonance width Γ and delay time Δt_{12} .

3.1.2. Unsymmetric potential functions. The potentials utilized in the study [11] just discussed were all symmetric functions. However, most chemical reactions do not possess this high degree of symmetry and, in addition, multiparticle three-dimensional quantal scattering calculations indicate that unsymmetric barriers can lead to new resonance phenomenon such as supernumerary transition states (see the O + H₂ discussion in Section 2.2.2). For these reasons, we were motivated to study one-dimensional quantal scattering by unsymmetric potential functions, with particular emphasis on potentials with two unequal local barrier maxima and their deformation to potentials having only one maximum. Such a study is described in detail in Ref. 12; we summarize its findings here.

In this second study [12], we considered potentials of the form

$$(3.4) \quad V(x) = \frac{V_1 e^{\beta_1(x-x_1)}}{(1 + e^{\beta_1(x-x_1)})^2} + \frac{V_2 e^{\beta_2(x-x_2)}}{(1 + e^{\beta_2(x-x_2)})^2}$$

with reduced mass $\mu = 6526.3m_e$. Parameters were chosen to roughly represent a one-dimensional model of the O + D₂ reaction. Two series of potential functions, all the form of eqn (3.4), were considered. In series 1, we focused on potential functions with two barrier maxima, taking $V_2 = 598.64$ meV, $\beta_1 = \beta_2 = 3a_0^{-1}$, $x_2 = -x_1 = 0.6a_0$, and V_1 variable. Nine different values of V_1 were considered and cases were labelled A-I. The potentials for representative cases A, C and I, with $V_1 = 598.64, 707.49$ and 870.75 meV, respectively, are shown in Figure 1. As we proceed from case A to case I, the lower local barrier maximum becomes less prominent.

In series 2, we continuously deformed the potentials so that eventually only one maximum appeared, rather than two. We took $V_1 = 870.75$ meV, $V_2 = 598.64$ meV, $x_2 = -x_1 = 0.6a_0$, and $\beta_1 = \beta_2 = \beta$ variable. Thirteen different values of β were considered and cases labelled I-U. (Case I is common to both series.) The potentials for representative cases K, N and T with $\beta = 2.80, 2.40$ and $1.80a_0^{-1}$, respectively, are shown in Figure 2.

Reaction probabilities P_{21} and reactive delay times Δt_{21} were computed. In addition, to further bring out structure in the reaction probability as a function of energy, we calculated the energy derivative of P_{21} by spline fitting the latter and analytically differentiating. Selected results are shown in Figures 1 and 2.

For all the potential cases, poles of the S matrix were located. The two resonances found in each case are characterized in the plots of the potential in Figures 1 and 2; the horizontal lines indicate values of ϵ_α and the number next to the horizontal line is the width Γ_α . The vertical lines in the other plots of Figures 1 and 2 indicate $\epsilon_\alpha - V_{\max}$.

In many of the delay time curves, there are two peaks and in such cases, there is very good agreement between the two values of ϵ_α and the energies of the local maxima of Δt_{21} for that particular case. (For example, notice how the vertical arrows in Figures 1 and 2 coincide with peaks in

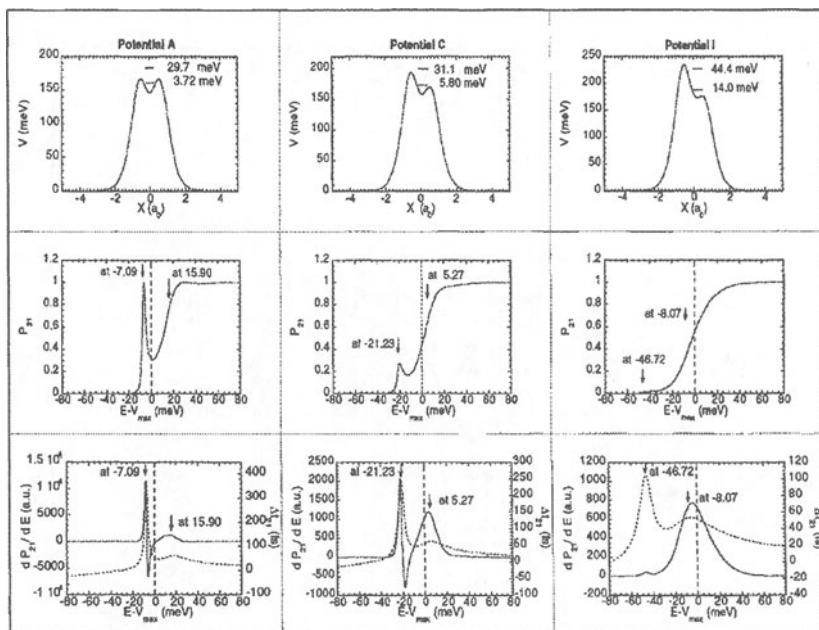


FIG. 1. Potential energy functions (top row), reaction probabilities (middle row), and derivatives of reaction probabilities and reactive delay times (bottom row) for cases A, C, and I of Section 3.1.2. In the top row, horizontal lines indicate the real parts ϵ_α of the resonance energies, and the numbers next to the lines are the widths Γ_α in meV. In the middle and bottom rows the location of V_{max} is shown as a dashed vertical line, and the values of ϵ_α are given (with arrows) relative to V_{max} in each case. Derivatives of the reaction probabilities are solid curves with the scale at the left, and delay times are dashed curves with the scale at the right. (Modified from Ref. 12.)

the reactive delay time.) Therefore, in such cases, we can associate each delay time peak with a resonance. In Figure 3 is plotted the value of the maximum in Δt_{21} versus the inverse of the width, $1/\Gamma$, of the closest resonance. We have also included results for $\alpha = 0 - 0.32$ and $0.68 - 1.60$ from Ref. 11 in addition to cases A, C, I, and K from Ref. 12. (Recall that for $\alpha = 0.49$ and cases N and T, two poles but only one maximum in the delay time were found.)

We now describe the main conclusions drawn from analyses of series 1 and 2, in turn.

For each of the potentials in series 1, two poles of the scattering matrix were located, and in general each resonance lies in the vicinity of a local potential barrier maximum (i.e. the value of ϵ_α is close to a local maximum in V .) The higher energy resonance (i.e. the one with larger ϵ_α) is always broader and is associated with a rise toward unity in the reaction probability and with a smaller peak in the reactive delay time. As the

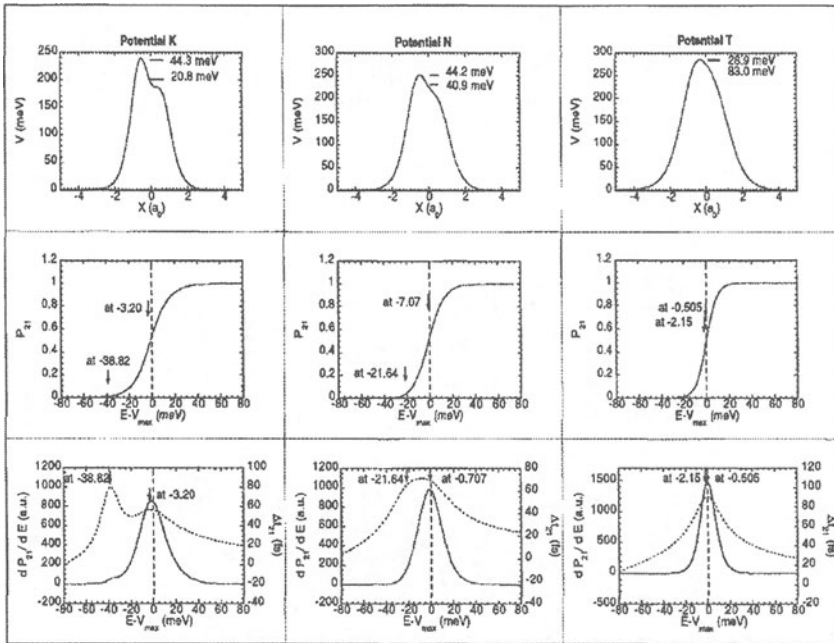


FIG. 2. Same as Fig. 1 except cases K, N, and T. (Modified from Ref. 12.)

resonance moves lower in energy relative to V_{max} , its width increases. The lower energy resonance, which lies in the vicinity of the lower local barrier maximum, has a smaller width and is associated with a larger peak in Δt_{21} . However, as we begin to deform the potential toward one having a single maximum, this resonance gets broader and its peak in the delay time gets smaller. In addition, its effect on the reaction probability is increasingly diminished; in case C, it is associated with a rise in P_{21} to only 0.27 and in case I, its effect on the reaction probability is really only discernible in the derivative curve dP_{21}/dE . Small rises in the reaction probability (to values significantly less than one) have also been observed in other model studies involving unsymmetric potentials [99,100].

For series 2, as we proceed from case I to T, the second potential maximum in $V(x)$ becomes a shoulder and then disappears, leaving only one maximum. Nonetheless, two poles of the scattering matrix are still located. Their values of ϵ_α approach one another and as a result the two peaks previously observed in Δt_{21} curves overlap more and more until they merge into one peak. While Γ of the higher energy resonance decreases, that of the lower energy resonance increases substantially; in case T, there is nearly a factor of 3 difference in widths.

Figure 3 clearly shows, for those potential cases in series 1 and 2 where

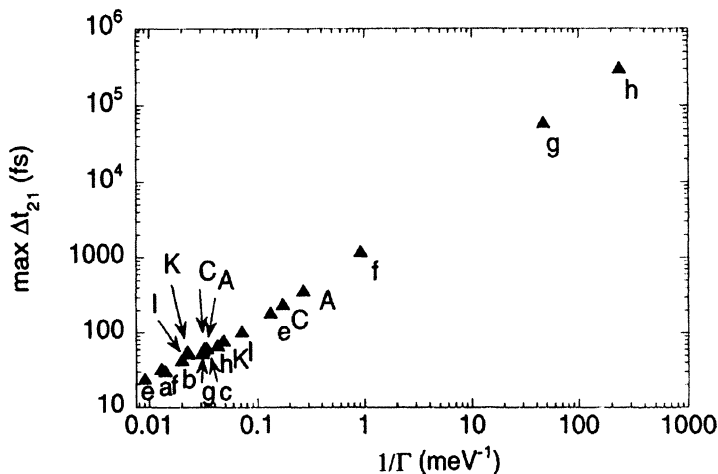


FIG. 3. Local maximum in the reactive delay time Δt_{21} versus the inverse of the width of the resonance associated with the delay time feature. The cases shown are $\alpha = 0$ (a), 0.17(b), 0.32(c), 0.68(e), 1.00(f), 1.45(g), and 1.60(h) of Section 3.1.1 and A, C, I, K of Section 3.1.2.

two peaks in Δt_{21} were observed, that the maximum delay time is inversely related to the width of the associated resonance. Cases N-T are not included in this figure because only one peak in Δt_{21} was observed in each case. However, even in these latter cases, there is an inverse relationship between the width of the *higher* energy resonance and the maximum delay time. (See Table 3 of Ref. 12.) While the width of the lower energy resonance increases, the higher energy resonance decreases in width, paralleling the increase in the maximum delay time. In addition there is an excellent correspondence between the value of ε_α of the higher energy resonance and the energy of maximum Δt_{21} . Thus, we conclude that when two resonances overlap significantly, it is the narrower (and higher energy) resonance which makes the dominant contribution to the delay time. We will revisit this point in Section 3.2 below.

The inverse relationship between the resonance width and the reactive delay time, clearly illustrated in Figure 3 for both symmetric and unsymmetric potential cases, can be elucidated in another manner. We have shown in Section 1.2 that for an isolated narrow resonance the reactive delay time will have a maximum at $E = \varepsilon_\alpha$, at which $\Delta t_{21}\Gamma_\alpha = 2\hbar$, eqn (1.16). This relationship is reminiscent of the time-energy uncertainty relation and we might expect that for broader resonances (such as barrier resonances) the product of the maximum reactive delay time and the resonance width will exceed $2\hbar$. In fact, we found that the very narrow resonances of potential (3.3) with $\alpha = 1.00 - 1.60$ are trapped-state resonances lying well below V_{\max} , and for these, the product equals 2.0, as it should for an INR.

For cases in series 1, the product falls between 2.1 and 2.3 for the narrower resonances and between 2.8 and 3.6 for the broader ones; for cases in series 2, it falls between 2.3 and 3.1 for the narrower resonances and between 3.7 and 4.2 for the broader ones [12]. The results agree very well with our expectations for broad and narrow resonances.

3.2. Strings of poles and the cumulative reaction probability.

The reaction probability P_{21} in the model one-dimensional studies is the analogue of the cumulative reaction probability in the three-dimensional quantal studies and, likewise, the energy derivative dP_{21}/dE is analogous to the density of reactive states. From accurate three-dimensional quantal calculations, we have concluded that quantized levels of the transition state control the chemical reactivity of a number of chemical reactions. We have interpreted these quantized transition states as barrier resonances, responsible for steplike rises in the CRP. In the chemical reactions discussed in Section 2, we find no evidence for trapped-state resonances affecting the overall CRP or density of reactive states. In a similar manner, we have seen in our model one-dimensional studies that broad barrier resonances are also responsible for the rise from zero towards unity in the reaction probability. For a relatively structureless potential barrier, like the simple Eckart potential of Section 3.1.1, we see that the reaction probability rises smoothly from zero to one and remains at unity. We have identified this as a resonance phenomenon. However, we have discussed above (Section 2.3) that a parabolic or approximately parabolic (e.g. an Eckart) barrier has a series of poles of the scattering matrix. We now address the relation between a string of poles and the reaction probability.

For the parabolic barrier of eqn (2.12), Atabek et al. [10] analytically solved the Schrödinger equation and found a series of poles accumulating at an energy corresponding to the top of the barrier with complex resonance energies given by eqn (2.24). They proceeded to try to characterize these resonances numerically by invoking some procedures used for traditional (i.e. trapped-state) resonances, such as the analysis of stabilization graphs [101] and the search for a wave packet of maximum lifetime [102]. An identical result for the poles of the S matrix (Siebert eigenvalues [16]) has been obtained by Seideman and Miller [92] in a treatment of the parabolic barrier. Eqn (2.24) for the string of poles also results from a naive continuation of the analytic results for a harmonic oscillator. For the potential of eqn (2.12) with, in this case, k_τ a *positive* force constant, the bound state eigenvalues, which are poles of S along the real energy axis, are $E_\tau + \hbar\omega_\tau(\nu + 1/2)$, with ω_τ given by eqn (2.15). If we let k_τ now be *negative*, which transforms the potential from a harmonic oscillator to a parabolic barrier, we get poles given by eqn (2.24).

Analytical results for the poles associated with scattering by an Eckart potential barrier were presented by Ryabov and Moiseyev [94]. For a sim-

ple, symmetric Eckart barrier of the form

$$(3.5) \quad V(x) = \frac{\alpha e^{\gamma x}}{(1 + e^{\gamma x})^2}$$

where α and γ are real constants with dimensions of energy and inverse length, respectively, there are a series of Siegert resonance states at complex energies

$$(3.6) \quad \bar{E}_\nu = \frac{\hbar^2 \gamma^2}{32\mu} \left[(1 + 2\nu) - i \sqrt{\frac{8\mu\alpha}{\hbar^2 \gamma^2} - 1} \right]^2$$

As for the parabolic barrier, the poles are labelled by a nonnegative integer ν and the widths of the resonances vary as $(2\nu + 1)$. A more complicated analytical formula for the complex resonance energies arises for the nonsymmetric Eckart potential [94]. It should be noted that the nonsymmetric potentials of Ref. 94 differ from those studied in Ref. 12; in the case of Ref. 94, the potentials possess one maximum but are asymmetric in their asymptotic energies [$V(x = +\infty) \neq V(x = -\infty)$]. The series of poles for the symmetric and nonsymmetric Eckart potentials were also located numerically using the complex coordinate method [103-108]. The authors found that the complex scaled Siegert eigenfunctions are square integrable and localized within the region of the potential barrier and, in addition, that they may be characterized by their number of nodes ν as for bound state wavefunctions.

In one relevant study [109], a string of poles of \mathbf{S} was also located for the radial potential $V_0 r^2 \exp(-\alpha r)$ using the complex coordinate method. (This potential was also studied by Bain et al. [108].) The locations of the poles in the complex energy plane relative to the potential barrier height were analysed. Pole strings have also been observed in a number of other studies [110,111]. The manner in which the series of Siegert resonance states line up in the complex energy plane for some general types of potentials has been discussed by Meyer [111] and Seideman and Miller [92]. Recent work in the mathematical literature is also concerned with the number and distribution of scattering poles [112].

The variation we have observed [11,12] in the widths of the resonances agrees nicely with the analytical and numerical studies of model one-dimensional barriers discussed above. In particular, we find that as the unsymmetric potential of eqn (3.4) is deformed from one having two local potential maxima to having only a single maximum, the ratio of the widths of the two resonances located is nearly 3. (For example, for case T in Figure 2, the ratio is 2.87.) For a parabolic barrier or a symmetric Eckart barrier, the ratio of the two narrowest resonances ($\nu = 0, 1$) is exactly 3.

Since passage over potential barriers can give rise to a series of poles of the scattering matrix, the next question to address is the effect this string of poles has on the reaction probability. Ryaboy and Moiseyev [94] proved

that the (cumulative) reaction probability for an Eckart potential barrier can be expressed entirely in terms of the Siegert poles in the S matrix, even though the energy dependence of P_{21} is structureless (it smoothly rises from zero to one). Likewise, Seideman and Miller [92] showed, using flux correlation functions [113,114], how the reaction probability for parabolic and Eckart barriers can be expressed in terms of Siegert eigenvalues. (In a related and earlier study, Atabek et al. [115] have shown that the scattering amplitude for single-channel scattering by a repulsive exponential potential can be accurately represented using a finite number of poles.) It is clear then that the rise in the reaction probability from 0 to 1 is due to a cumulative effect of the entire string of poles. Whereas an isolated narrow trapped-state resonance causes the reaction probability to rapidly vary from 0 to 1 and then back to 0, the reaction probability upon passage over a simple potential barrier (such as a simple Eckart potential) rises smoothly from 0 to 1 but does not return to 0 because of the cumulative effect of the string of broad and hence overlapping resonances.

However, it is important to reemphasize a point made earlier. The quantal three-dimensional studies described in Section 2 suggest that, when resonances are broad and overlapping, many features of the behavior of the cumulative reaction probability and density of reactive states can be understood in terms of the pole closest to the real energy axis (the $\nu = 0$ member of the pole sequence). We have discussed several examples of the utility of this suggestion in Section 2.3. In addition, both in our work on three-body reactions in the real three-dimensional world described in Section 2 and in our work on model one-dimensional unsymmetric potential functions described in Section 3.1.2, we concluded that when resonances overlap significantly, it is the narrowest one which makes the dominant contribution to the delay time. The nearest pole to the real energy axis is thus useful for understanding the dynamics in real time, an issue that is becoming increasingly important due to recent advances in femtosecond spectroscopy [116].

4. Concluding remarks. Analytical formulas characterizing isolated narrow resonances are well known. However, resonances that are encountered in molecular collisions usually are not well described by the INR formulas; in particular, we have given a number of examples from the literature where the sum of the partial widths does not equal the total resonance width.

A chemically important example of a type of resonance that is not expected to follow the isolated narrow resonance formulas is a quantized transition state resonance. These broad resonances have been shown, by analysis of the accurate quantum mechanical cumulative reaction probability and its energy derivative, to control chemical reactivity in a number of three-dimensional chemical reactions by acting as dynamical bottlenecks in phase space that gate the reactive flux from reactants to products. These

transition state resonances, also called barrier resonances, do not differ in kind from conventional isolated narrow trapped-state resonances (i.e. both are poles of the scattering matrix); this has been demonstrated by one-dimensional quantal studies in which barrier resonances have been shown to transform continuously into trapped-state resonances by varying the potential energy function. In general, barrier resonances have larger widths (and are consequently associated with shorter delay times) than trapped-state resonances.

When the quantum mechanical description of a chemical reaction becomes more complete, it often becomes desirable or even necessary to use the language of resonance theory. The interpretation of transition states as resonances has been put to several practical uses. First, it allows us to compute the collision lifetime $\Delta\tau$ from the resonance width; $\Delta\tau$ values computed in this manner have been seen to compare favorably to those computed from the phase of accurate S matrix elements without resonance theory or transition state theory. Secondly, we can obtain complex spectroscopic constants for the quantized transition states by analogy to the well known procedure for obtaining (real) spectroscopic constants for bound states. Thirdly, by analysing channel-selected densities of reactive states, we can acquire information regarding the partial widths of these barrier resonances. This allows us to determine quantitatively which reactant states contribute to the reactive flux passing through a particular level of the transition state. In addition, the characterization of transition states as resonances has been used in a reformulation of variational transition state theory to compute anharmonic transition state energy levels [93].

The identification of transition states as reactive scattering resonances has been shown [117] to also result from application of a complex scaling transformation to the reaction coordinate of a chemical reaction. This analysis leads to a precise definition of the resonance width operator, whose expectation values are resonance lifetimes.

The levels of the transition state have been assigned stretch (v_1) and bend (v_2) quantum numbers for modes orthogonal to the reaction coordinate. The quantum number v_3 , corresponding to the unbound motion along the reaction coordinate, appears to be missing in the $[v_1 v_2^K]$ assignments; however, when the transition state is treated properly as a quantum mechanical resonance, this quantum number reappears and is related to the quantum number ν used to label each resonance in the string of poles associated with passage over a one-dimensional potential barrier. We suggest that the "missing" quantum number in the transition state assignment be taken as $\nu = 0$, corresponding to the pole in the one-dimensional study string of poles that is nearest to the real energy axis. Our three-dimensional and one-dimensional studies suggest that it is the $\nu = 0$ pole that is most useful for understanding the chemical dynamics in real time.

Quantum mechanical scattering by one-dimensional potential energy functions has provided further insight into the nature of transition state,

or barrier, resonances. In conclusion, we briefly point out how our one-dimensional model studies on unsymmetric potential energy functions can help us better understand the conclusions drawn from our multidimensional quantal studies of the asymmetric $O + H_2$ reaction. As described above, the three-dimensional quantal calculations suggest that reactant-like dynamical bottlenecks exert significant control on $O + H_2$ chemical reactivity; these bottlenecks are variational transition states associated with the global maxima of vibrationally adiabatic curves. In addition, there are product-like dynamical bottlenecks (supernumerary transition states) that also affect the cumulative reaction probability and density of reactive states. However, other product-like transition states do not appear to influence the overall CRP (such as product-like $[10^0]$.) We find in our model studies of one-dimensional unsymmetric potentials having two potential maxima that the resonance in the vicinity of the global potential maximum is associated with the rise in the reaction probability toward one; this resonance behaves like the variational transition state. The resonance in the vicinity of the lower local potential maximum sometimes appears to significantly influence P_{21} (as in case C of Section 3.1.2) like a supernumerary transition state and at other times appears to have very little influence (see case K in the same section). Although it is clear that comparison between model one-dimensional studies and quantal three-dimensional studies has its limitations, it is encouraging to see that some aspects of the three-dimensional results can be better understood in light of the one-dimensional studies. In the spirit of the present workshop we would like to suggest that the subject of broad overlapping resonances and especially barrier resonances provides a fertile area for further mathematical analysis that could be of great use in multiparticle scattering theory.

Acknowledgment: We gratefully acknowledge useful conversations with David Chatfield, Brian Kendrick, Claude Mahaux, David Schwenke, and Deborah Watson. This work was supported by the National Science Foundation, by the donors of The Petroleum Research Fund, administered by the American Chemical Society, by an Indiana University Purdue University Fort Wayne Summer Faculty Research Grant, and by a Purdue Research Foundation Summer Faculty Grant. Computational resources were provided by the Minnesota Supercomputer Institute and the Chemistry Department at IPFW.

Appendix I

Accurate quantum mechanical cumulative reaction probabilities and densities of reactive states for three-dimensional chemical reactions such as those discussed in Section 2.2 were obtained by performing converged quantum dynamics calculations. After removing the center-of-mass motion, this leaves 6 degrees of freedom. The scattering calculations were carried out by expanding the wavefunction in a multiple-arrangement basis set [118-122]

and finding the basis set coefficients by linear algebraic methods utilizing a variational principle. Either the generalized Newton variational principle [15,123-126] or the outgoing wave variational principle [127-130] was used to obtain elements of the scattering matrix that are stationary with respect to small variations in the wavefunction. Details of the calculations are presented in previously published work [125,126,130-133]. We emphasize that the state-to-state reaction probabilities are very well converged with respect to numerical and basis set parameters; this is of crucial importance since densities of reactive states are obtained by numerical differentiation of CRPs with respect to energy, and the errors in the CRP must be small for the numerical derivatives to be smooth.

Appendix II

In this appendix we briefly describe the computational methods used in Refs. 11 and 12 for solution of the Schrödinger equation (3.1) describing two-channel, one-dimensional scattering. The scattering boundary conditions are

$$(II.1a) \quad \psi \underset{x \rightarrow -\infty}{\sim} \frac{N_-}{\sqrt{k_-}} [C \exp(-ik_-x) + D \exp(ik_-x)]$$

$$(II.1b) \quad \psi \underset{x \rightarrow +\infty}{\sim} \frac{N_+}{\sqrt{k_+}} [A \exp(-ik_+x) + B \exp(ik_+x)]$$

where N_{\pm} is an arbitrary normalization factor, and asymptotic wave numbers k_{\pm} are given by

$$(II.2) \quad k_{\pm} = \sqrt{2\mu(E - V_{\pm\infty})}/\hbar$$

where $V_{\pm\infty}$ are the limits at $x = \pm\infty$ of $V(x)$. The S matrix relates the incoming wave coefficients A and D and the outgoing wave coefficients B and C :

$$(II.3) \quad \begin{pmatrix} C \\ B \end{pmatrix} = \begin{pmatrix} S_{11} & S_{12} \\ S_{21} & S_{22} \end{pmatrix} \begin{pmatrix} D \\ A \end{pmatrix}$$

We used two different numerical methods to directly search for poles of \mathbf{S} at complex energies. The first method [11,12] located most of the resonances studied but had difficulty characterizing very broad resonances. A second method [12] was used to locate the broadest resonances.

Before describing each method, we note that we considered potentials for which $V_{+\infty} = V_{-\infty} = 0$ and thus $k_+ = k_- = k$. We also set $N_{\pm} = \sqrt{k}$ for convenience.

In the first method, we transformed the second-order, complex differential equation (3.1) into four coupled first-order real differential equations

which we then integrated directly. In particular, if we consider a wave incident only from $x > 0$, we can set $D = 0$ and thus, with $C = 1$ to normalize the solution, we know the solution of eqn (3.1) as $x \rightarrow -\infty$. This solution is then numerically propagated from a large negative value of x , $-a_1$, to a large positive value of x , a_2 , using a variable stepsize Gear backward difference integrator [134] subroutine from the International Mathematical and Statistical Library (IMSL) [135]. From the solution at a_2 , the coefficients A and B are computed and then S_{22} and S_{12} determined using eqn II.3. In a similar manner, we can compute the remaining two S matrix elements by again setting $D = 0$ and $C = 1$ but solving the Schrödinger equation with the potential $V(-x)$ rather than $V(x)$. The numerical parameters required for the numerical integration were varied until the scattering matrix elements were converged to better than 0.1%.

The second method we used to both locate the very broad resonances as well as check the results obtained from the first method is based on the technique of invariant embedding [136]. Equivalent to solving the second-order, linear eqn (3.1) subject to the above boundary conditions is to solve the following first-order, nonlinear initial value problem for the function $S(x)$ [137]:

$$(II.4a) \quad \frac{dS}{dx} = 2ikS(x) + \frac{1}{2ik}U(x)[1 + S(x)]^2$$

$$(II.4b) \quad S(-a_1) = 0$$

with $U(x) = 2\mu V(x)/\hbar^2$. Scattering matrix elements are then given by

$$(II.5a) \quad S_{22} = S(a_2) \exp(-2ika_2)$$

$$(II.5b) \quad S_{12} = \exp\left(\frac{1}{2ik} \int_{-a_1}^{a_2} dx U(x)[1 + S(x)]\right).$$

The first-order equation (II.4a) is transformed into two real, first-order coupled differential equations and the solution II.4b is propagated numerically from $-a_1$ to a_2 using the IMSL Gear integrator. S_{22} is computed via eqn II.5a and S_{12} is computed from a Simpson's rule [138] evaluation of the integral in II.5b.

Poles in the scattering matrix corresponding to resonances were located by numerically searching for zeroes in $1/S_{ji}$ in the complex energy plane. To accomplish this task, we used a modified IMSL subroutine which invoked Muller's method [138] for quadratic interpolation among three points to find the next estimate of the root. The search was typically stopped when the relative difference in two successive approximations to the root was smaller than 10^{-10} .

Transmission and reflection coefficients were computed at real energies from converged scattering matrix elements via eqn (3.2). Delay times Δt_{ij} defined by eqn (1.14) were also obtained by the method [33] of fitting

scattering matrix elements at three consecutive real energies to

$$(II.6) \quad S_{ji}(E) = (c_1 + c_2 E + c_3 E^2) \times \exp[i(c_4 + c_5 E + c_6 E^2)]$$

where c_n are real fitting parameters. The delay time at the central energy of the triad was then obtained by

$$(II.7) \quad \Delta t_{ij}(E) = \hbar(c_5 + 2c_6 E).$$

REFERENCES

- [1] J. R. Taylor, *Scattering Theory: The Quantum Theory of Nonrelativistic Collisions*, Krieger, Malabar, FL, 1983, p. 238, (a) p. 407.
- [2] H.S. Taylor, G.V. Nazarov, and A. Golebiewski, *J. Chem. Phys.* 45: 2872, 1966.
- [3] B. C. Garrett, D. G. Truhlar, R. S. Grev, G. C. Schatz, and R. B. Walker, *J. Phys. Chem.* 85: 3806, 1981.
- [4] J. Simons, *ACS Symp. Ser.* 263: 3, 1984.
- [5] H. Feshbach, *Ann. Phys. (N. Y.)* 19: 287, 1962.
- [6] N. Abusalbi, D. J. Kouri, M. Baer, and E. Pollak, *J. Chem. Phys.* 82: 4500, 1985.
- [7] R. D. Levine and S.-f. Wu, *Chem. Phys. Lett.* 11: 557, 1971.
- [8] S. A. Cuccaro, P. G. Hipes, and A. Kuppermann, *Chem. Phys. Lett.* 157: 440, 1989.
- [9] Z. C. Kuruoglu and D. A. Micha, *Int. J. Quantum Chem. Symp.* 23: 103, 1989.
- [10] O. Atabek, R. Lefebvre, M. Garcia Sucre, J. Gomez-Llorente, and H. Taylor, *Int. J. Quantum Chem.* 40: 211, 1991.
- [11] R. S. Friedman and D. G. Truhlar, *Chem. Phys. Lett.* 183: 539, 1991.
- [12] R. S. Friedman, V. D. Hullinger, and D. G. Truhlar, *J. Phys. Chem.* 99: 3184, 1995.
- [13] A. Bohm, *Quantum Mechanics: Foundations and Applications*, 3rd ed., Springer-Verlag, New York, 1993, p. 452.
- [14] *Resonances*, E. Brändas and N. Elander (eds.) [*Lecture Notes in Physics*, Vol. 325], Springer-Verlag, Berlin, 1989.
- [15] R. G. Newton, *Scattering Theory of Particles and Waves*, 2nd ed., Springer-Verlag, New York, 1982, Section 11.2 and Chapter 16 for resonances as poles of the S matrix and Section 11.3 for variational principles.
- [16] A. J. F. Siegert, *Phys. Rev.* 56: 750, 1939.
- [17] B. Simon, *Int. J. Quantum Chem.* 14: 529, 1978.
- [18] G. A. Hagedorn, *Commun. Math. Phys.* 65: 181, 1979.
- [19] D. C. Chatfield, R. S. Friedman, D. G. Truhlar, B. C. Garrett, and D. W. Schwenke, *J. Am. Chem. Soc.* 113: 486, 1991.
- [20] D. C. Chatfield, R. S. Friedman, D. G. Truhlar, and D. W. Schwenke, *Faraday Discuss. Chem. Soc.* 91: 289, 1991.
- [21] D. C. Chatfield, R. S. Friedman, D. W. Schwenke, and D. G. Truhlar, *J. Phys. Chem.* 96: 2414, 1992.
- [22] D. G. Truhlar, C. A. Mead, and M. A. Brandt, *Adv. Chem. Phys.* 33: 296, 1975.
- [23] A. M. Lane and R. G. Thomas, *Rev. Mod. Phys.* 30: 257, 1958.
- [24] J. Humblet and L. Rosenfeld, *Nucl. Phys.* 26: 529, 1961. J. Humblet and L. Rosenfeld, *Nucl. Phys.* 31: 544, 1962. J. Humblet, in *Fundamentals in Nuclear Theory* (Lectures Presented at and International Course, Trieste, 3 Oct.-16 Dec. 1966), A. de-Shalit and C. Villi, eds., International Atomic Energy Agency, Vienna, 1967, p. 369.
- [25] H. A. Weidenmüller, *Ann. Phys. (N.Y.)* 28: 60, 1964; 29: 378, 1964. See also C. Mahaux and H. A. Weidenmüller, *Shell-Model Approach to Nuclear Reactions*, North-Holland, Amsterdam, 1969.
- [26] P. A. Moldauer, *Phys. Rev.* 135B: 642, 1964.

- [27] D. W. Schwenke and D. G. Truhlar, *J. Chem. Phys.* 87: 1095, 1987.
- [28] A. Bohm, *Quantum Mechanics: Foundations and Applications*, 3rd ed., Springer-Verlag, New York, 1993, p. 549.
- [29] D. K. Watson, *Phys. Rev. A* 34: 1016, 1986. D. K. Watson, *J. Phys. B* 19: 293, 1986.
- [30] R. K. Nesbet, *Adv. At. Mol. Phys.* 13: 315, 1977. A. Hazi, *Phys. Rev. A* 19: 920, 1979.
- [31] H.A. Weidenmüller, *Phys. Lett.* 24B: 441, 1967.
- [32] F. T. Smith, *Phys. Rev.* 118: 349, 1960.
- [33] M. Zhao, M. Mladenovic, D. G. Truhlar, D. W. Schwenke, O. Sharafeddin, Y. Sun, and D. J. Kouri, *J. Chem. Phys.* 91: 5302, 1989.
- [34] R. H. Dalitz and G. Rajasekaran, *Phys. Lett.* 7: 373, 1963. R. J. Eden and J.R. Taylor, *Phys. Rev. B* 133: 1575, 1964. A. Herzenberg and D. Ton-That, *J. Phys. B* 8: 426, 1975.
- [35] C. J. Ashton, M. S. Child, and J. M. Hutson, *J. Chem. Phys.* 78: 4025, 1982.
- [36] H. Feshbach, *Ann. Phys. (N. Y.)* 43: 410, 1967.
- [37] B. W. Shore, *Phys. Rev.* 171: 43, 1968.
- [38] A. Mondragón and E. Hernández, *J. Phys. A* 26, 5595, 1993.
- [39] M. Desouter-Lecomte, J. Lievin, and V. Brems, *J. Chem. Phys.* 103: 4524, 1995. M. Desouter-Lecomte and V. Jacques, *J. Phys. B* 28: 3225, 1995.
- [40] E. P. Wigner and L. Eisenbud, *Phys. Rev.* 72: 29, 1947.
- [41] G. Beck and H. M. Nussenzweig, *Nuovo Cimento* 16: 416, 1960.
- [42] M. Desouter-Lecomte, and F. Culot, *J. Chem. Phys.* 98: 7819, 1993.
- [43] B. C. Garrett, D.W. Schwenke, R.T. Skodje, D. Thirumalai, T.C. Thompson, and D. G. Truhlar, *A.C.S. Symp. Ser.* 263: 375, 1984.
- [44] M. V. Basilevsky and V. M. Ryaboy, *Int. J. Quantum Chem.* 19: 611, 1981.
- [45] M. V. Basilevsky and V. M. Ryaboy, *Chem. Phys.* 86: 67, 1984.
- [46] C. W. McCurdy and T. N. Rescigno, *Phys. Rev. A* 20: 2346, 1979.
- [47] D. W. Schwenke, *Theor. Chim. Acta* 74: 381, 1988.
- [48] H. Eyring, *J. Chem. Phys.* 3: 107, 1935.
- [49] E. Wigner, *Trans. Faraday Soc.* 34: 29, 1938.
- [50] M. M. Kreevoy and D. G. Truhlar, *Transition state theory, in Investigation of Rates and Mechanisms of Reactions (C. F. Bernasconi, ed.) [Techniques of Chemistry, 4th ed., A. Weissberger (ed.)]*, John Wiley & Sons, New York, 1986, Part I, pp. 13-95.
- [51] S. C. Tucker and D. G. Truhlar, in *New Theoretical Concepts for Understanding Organic Reactions (J. Bertrán and I. G. Csizmadia, Eds.)*, Kluwer, Dordrecht, 1989, pp. 291-346.
- [52] J. C. Polanyi and R. J. Wolf, *J. Chem. Phys.* 75: 5951, 1981. H. R. Mayne, R. A. Poirier, and J. C. Polanyi, *J. Chem. Phys.* 80: 4025, 1984. H. R. Mayne, J. C. Polanyi, N. Sathyamurthy, and S. Raynor, *J. Phys. Chem.* 88: 4064, 1984. J. C. Polanyi, M. G. Prisant, and J. S. Wright, *J. Phys. Chem.* 91: 4727, 1987.
- [53] R. A. Marcus and O. K. Rice, *J. Phys. Colloid Chem.* 55: 894, 1951. R. A. Marcus, *J. Chem. Phys.* 20: 359, 1952.
- [54] R. A. Marcus, *J. Chem. Phys.* 45: 2138, 1966.
- [55] H. M. Rosenstock, M. B. Wallenstein, A. L. Wahrhaftig, and H. Eyring, *Proc. Natl. Acad. Sci. USA* 38: 667, 1952.
- [56] J. L. Magee, *Proc. Natl. Acad. Sci. USA* 38: 764, 1952.
- [57] B. C. Garrett and D. G. Truhlar, *J. Phys. Chem.* 83: 1052, 1979.
- [58] B. C. Garrett and D. G. Truhlar, *J. Phys. Chem.* 83: 1079, 1979; *Errata:* 84: 682, 1980; 87: 4553, 1983.
- [59] W. H. Miller, *J. Chem. Phys.* 62: 1899, 1975.
- [60] F. T. Smith, *J. Chem. Phys.* 36: 248, 1962.
- [61] E. Wigner, *J. Chem. Phys.* 5: 720, 1937.
- [62] J. Horiuti, *Bull. Chem. Soc. Japan* 13: 210, 1938.
- [63] J. C. Keck, *Advan. Chem. Phys.* 13: 85, 1967.

- [64] D. G. Truhlar and B. C. Garrett, *Annu. Rev. Phys. Chem.* 35: 159, 1984.
- [65] D. G. Truhlar, A. D. Isaacson, and B. C. Garrett, in *Theory of Chemical Reaction Dynamics* (M. Baer, ed.), CRC Press, Boca Raton, FL, 1985, Vol. 4, pp. 65-137.
- [66] K. Haug, D. W. Schwenke, D. G. Truhlar, Y. Zhang, J. Z. H. Zhang, and D. J. Kouri, *J. Chem. Phys.* 87: 1892, 1987.
- [67] J. M. Bowman, *Chem. Phys. Lett.* 141: 545, 1987.
- [68] D. C. Chatfield, R. S. Friedman, G. C. Lynch, D. G. Truhlar, and D. W. Schwenke, *J. Chem. Phys.* 98: 342, 1993.
- [69] S. L. Mielke, G. C. Lynch, D. G. Truhlar, and D. W. Schwenke, *J. Phys. Chem.* 98: 8000, 1994.
- [70] D. C. Chatfield, R. S. Friedman, S. L. Mielke, D. W. Schwenke, G. C. Lynch, T. C. Allison, and D. G. Truhlar, *Computational Spectroscopy of the Transition State*, in *Dynamics of Molecules and Chemical Reactions*, edited by R. E. Wyatt and J. Z. H. Zhang (Marcel Dekker, New York, 1996), pp. 323-386.
- [71] J. D. Kress and E. F. Hayes, *J. Chem. Phys.* 97: 4881, 1992. G. C. Lynch, P. Halvick, M. Zhao, D. G. Truhlar, C.-h. Yu, D. J. Kouri, and D. W. Schwenke, *J. Chem. Phys.* 94: 7150, 1991.
- [72] T. C. Allison, S. L. Mielke, D. W. Schwenke, G. C. Lynch, M. S. Gordon, and D. G. Truhlar, *Die Photochemischen Bildung des Chlorwasserstoffs. Dynamics of Cl + H₂F HCl + H on a New Potential Energy Surface: The Photosynthesis of Hydrogen Chloride Revisited 100 Years after Max Bodenstein*, in *Gas-Phase Chemical Reaction Systems: Experiments and Models 100 Years after Max Bodenstein*, edited by J. Wolfrum, H.-R. Volpp, R. Rannacher, J. Warnatz (Springer Series in Chemical Physics, Berlin, 1996), pp. 111-124.
- [73] D. C. Chatfield, R. S. Friedman, G. C. Lynch, and D. G. Truhlar, *Faraday Discuss. Chem. Soc.* 91: 398, 1991. D. C. Chatfield, R. S. Friedman, G. C. Lynch, and D. G. Truhlar, *J. Phys. Chem.* 96: 57, 1992. The cumulative reaction probabilities were presented in: G.C. Schatz, *J. Chem. Phys.* 90: 3582, 1989. G. C. Schatz, *J. Chem. Phys.* 90: 4847, 1989. G. C. Schatz, *J. Chem. Soc. Faraday Trans.* 86: 1729, 1990.
- [74] Z. Darakjian, E. F. Hayes, G. A. Parker, E. A. Butcher, and J. D. Kress, *J. Chem. Phys.* 95: 2516, 1991. Erratum: 101: 9203, 1994. S. J. Klippenstein and J. D. Kress, *J. Chem. Phys.* 96: 8164, 1992.
- [75] J. D. Kress, *J. Chem. Phys.* 95: 8673, 1991. J. D. Kress and S. J. Klippenstein, *Chem. Phys. Lett.* 195: 513, 1992. J. D. Kress, R. B. Walker, E. F. Hayes, and P. Pendergast, *J. Chem. Phys.* 100: 2728, 1994.
- [76] R. T Pack, E. A. Butcher, and G. A. Parker, *J. Chem. Phys.* 99: 9310, 1993. R. T Pack, E. A. Butcher, and G. A. Parker, *J. Chem. Phys.* 102: 5998, 1995. C. Leforestier and W. H. Miller, *J. Chem. Phys.* 100: 733, 1994.
- [77] M. J. Davis, H. Koizumi, G. C. Schatz, S. E. Bradforth, and D. M. Neumark, *J. Chem. Phys.* 101: 4708, 1994.
- [78] D. G. Truhlar and R. E. Wyatt, *Annu. Rev. Phys. Chem.* 27: 1, 1976.
- [79] C. A. Mead, in *Mathematical Frontiers in Computational Chemical Physics* (D. G. Truhlar, ed.), Springer-Verlag, New York, 1988, p. 1.
- [80] A. J. C. Varandas, F. B. Brown, C. A. Mead, D. G. Truhlar, and N. C. Blais, *J. Chem. Phys.* 86: 6258, 1987.
- [81] E. C. Kemble, *The Fundamental Principles of Quantum Mechanics with Elementary Applications*, Dover, New York, 1958, p. 109.
- [82] G. Herzberg, *Infrared and Raman Spectra of Polyatomic Molecules* [Molecular Spectra and Molecular Structure, Vol. II], Van Nostrand Reinhold, New York, 1945, pp. 15, 75, 205.
- [83] M. A. Eliason and J. O. Hirschfelder, *J. Chem. Phys.* 30: 1426, 1959.
- [84] L. Hofacker, *Z. Naturforsch.* 18a: 607, 1963.
- [85] D. G. Truhlar, *J. Chem. Phys.* 53: 2041, 1970.
- [86] D. G. Truhlar and A. Kuppermann, *J. Amer. Chem. Soc.* 93: 1840, 1971.

- [87] B. C. Garrett, D. G. Truhlar, R. S. Grev, and A. W. Magnuson, *J. Phys. Chem.* 84: 1730, 1980. Errata: 87: 4554, 1983.
- [88] R. A. Marcus, *J. Chem. Phys.* 45: 4493, 1965.
- [89] G. C. Lynch, P. Halvick, D. G. Truhlar, B. C. Garrett, D. W. Schwenke, and D. J. Kouri, *Z. Naturforsch.* 44a: 427, 1989.
- [90] B. R. Johnson and N. W. Winter, *J. Chem. Phys.* 66: 4116, 1977.
- [91] G. C. Schatz, *J. Chem. Phys.* 83: 5677, 1985.
- [92] T. Seideman and W. H. Miller, *J. Chem. Phys.* 95: 1768, 1991.
- [93] D. G. Truhlar and B. C. Garrett, *J. Phys. Chem.* 96: 6515, 1992.
- [94] V. Ryaboy and N. Moiseyev, *J. Chem. Phys.* 98: 9618, 1993.
- [95] A. Kuppermann, in *Potential Energy Surfaces and Dynamics Calculations* (D. G. Truhlar, ed.), Plenum, New York, 1981, p. 375.
- [96] A. Messiah, *Quantum Mechanics*, Wiley, New York, 1966, p. 85.
- [97] D. G. Truhlar and A. Kuppermann, *J. Am. Chem. Soc.* 93: 1840, 1971.
- [98] C. Eckart, *Phys. Rev.* 35: 1303, 1930.
- [99] V. A. Mandelshtam and H. S. Taylor, *J. Chem. Phys.* 99: 222, 1993.
- [100] V. Ryaboy and R. Lefebvre, *J. Chem. Phys.* 99: 9547, 1993.
- [101] A. U. Hazi and H. S. Taylor, *Phys. Rev. A* 1: 1109, 1970.
- [102] D. G. Truhlar, *Chem. Phys. Lett.* 26: 377, 1974.
- [103] J. Nuttall and H. L. Cohen, *Phys. Rev.* 188: 1542, 1969.
- [104] E. Balslev and J. M. Combes, *Commun. Math. Phys.* 22: 280, 1971.
- [105] B. Simon, *Commun. Math. Phys.* 27: 1, 1972; *Ann. Math.* 97: 247, 1973.
- [106] B. R. Junker, *Adv. At. Mol. Phys.* 18: 207, 1982. B. R. Junker and C. L. Huang, *Phys. Rev. A* 18: 313, 1978.
- [107] N. Moiseyev, *Isr. J. Chem.* 31: 211, 1991.
- [108] R. A. Bain, J. N. Bardsley, B. R. Junker, and C. V. Sukumar, *J. Phys. B.* 7: 2189, 1974.
- [109] O. Atabek and R. Lefebvre, *Chem. Phys. Lett.* 84: 233, 1981.
- [110] See, for examples, N. Moiseyev, P. R. Certain, and F. Weinhold, *Mol. Phys.* 36: 1613, 1978. H. J. Korsch, H. Laurent, and R. Möhlenkamp, *Mol. Phys.* 43: 1441, 1981; *J. Phys. B* 15: 1, 1982; *J. Phys. B* 15: L559, 1982. M. Rittby, N. Elander, and E. Brändas, *Phys. Rev. A* 24: 1635, 1981; *Mol. Phys.* 45: 553, 1982. H-D. Meyer and O. Walter, *J. Phys. B* 15: 3647, 1982.
- [111] H-D. Meyer, *J. Phys. B* 16: 2265, 1983.
- [112] J. Sjöstrand and M. Zworski, *Commun. Partial Diff. Eq.* 17: 1021, 1992. R. Froese and M. Zworski, *Duke Math. J.* 72: 275, 1993. J. Sjöstrand and M. Zworski, *Commun. Partial Diff. Eq.* 18: 847, 1993. J. Sjöstrand and M. Zworski, *J. Funct. Anal.* 123: 336, 1994. J. Sjöstrand, *Int. J. Quantum Chem.* 31: 733, 1987. M. Zworski, *J. Funct. Anal.* 73: 277, 1987; 89: 370, 1989. M. Zworski, *Duke Math. J.* 59: 311, 1989. J. Sjöstrand, *Duke Math. J.* 60: 1, 1990.
- [113] T. Yamamoto, *J. Chem. Phys.* 33: 281, 1960.
- [114] W. H. Miller, S. D. Schwartz, and J. W. Tromp, *J. Chem. Phys.* 79: 4889, 1983. T. Seideman and W. H. Miller, *J. Chem. Phys.* 96: 4412, 1992.
- [115] O. Atabek, R. Lefebvre, and M. Jacon, *J. Phys. B* 15: 2689, 1982.
- [116] A. H. Zewail and R. B. Bernstein, *Chem. Eng. News* 66: 24, Nov. 7, 1988; L. R. Khundkar and A. H. Zewail, *Annu. Rev. Phys. Chem.* 41: 15, 1990; A. H. Zewail, *Faraday Discuss. Chem. Soc.* 91: 207, 1991; A. H. Zewail, *J. Phys. Chem.* 97: 12427, 1993; A. Materny, J. L. Herek, P. Cong, and A. H. Zewail, *J. Phys. Chem.* 98: 3352, 1994.
- [117] M. Zhao and S. A. Rice, *J. Phys. Chem.* 98: 3444, 1994.
- [118] M. J. Seaton, *Philos. Trans. Roy. Soc. London A* 245: 469, 1953.
- [119] H. S. W. Massey, *Rev. Mod. Phys.* 28: 199, 1956.
- [120] D. A. Micha, *Arkiv Fys.* 30: 411, 1965.
- [121] W. H. Miller, *J. Chem. Phys.* 50: 407, 1969.
- [122] D. G. Truhlar, J. Abdallah, Jr., and R. L. Smith, *Adv. Chem. Phys.* 25: 211, 1974. D. G. Truhlar and J. Abdallah, Jr., *Phys. Rev. A* 9: 297, 1974.

- [123] G. Staszewska and D. G. Truhlar, *J. Chem. Phys.* 86: 2793, 1987.
- [124] D. W. Schwenke, K. Haug, D. G. Truhlar, Y. Sun, J. Z. H. Zhang, and D. J. Kouri, *J. Phys. Chem.* 91: 6080, 1987.
- [125] D. W. Schwenke, K. Haug, M. Zhao, D. G. Truhlar, Y. Sun, J. Z. H. Zhang, and D. J. Kouri, *J. Phys. Chem.* 92: 3202, 1988.
- [126] D. W. Schwenke, M. Mladenovic, M. Zhao, D. G. Truhlar, Y. Sun, and D. J. Kouri, in *Supercomputer Algorithms for Reactivity Dynamics and Kinetics of Small Molecules* (A. Laganà, ed.), Kluwer, Dordrecht, 1989, p. 131.
- [127] L. Schlessinger, *Phys. Rev.* 167: 1411, 1968.
- [128] Y. Sun, D. J. Kouri, D. G. Truhlar, and D. W. Schwenke, *Phys. Rev. A* 41: 4857, 1990.
- [129] Y. Sun, D. J. Kouri, and D. G. Truhlar, *Nucl. Phys. A* 508: 41c, 1990.
- [130] D. W. Schwenke, S. L. Mielke, and D. G. Truhlar, *Theor. Chim. Acta* 79: 241, 1991.
- [131] J. Z. H. Zhang, D. J. Kouri, K. Haug, D. W. Schwenke, Y. Shima, and D. G. Truhlar, *J. Chem. Phys.* 88: 2492, 1988.
- [132] D. W. Schwenke and D. G. Truhlar, in *Computing Methods in Applied Sciences and Engineering* (R. Glowinski and A. Lichnewsky, eds.), SIAM, Philadelphia, 1990, p. 291. S. L. Mielke, D. G. Truhlar, and D. W. Schwenke, *J. Chem. Phys.* 95: 5930, 1991.
- [133] G. J. Tawa, S. L. Mielke, D. G. Truhlar, and D. W. Schwenke, *J. Chem. Phys.* 100: 5751, 1994. G.J. Tawa, S.L. Mielke, D.G. Truhlar, and D.W. Schwenke, in *Advances in Molecular Vibrations and Collision Dynamics*, Vol. 2B (J.M. Bowman, ed.), JAI, Greenwich, CT, 1994, pp. 45-116.
- [134] C.W. Gear, *Numerical Initial Value Problems in Ordinary Differential Equations*, Prentice-Hall, Englewood Cliffs, 1971.
- [135] *International Mathematical and Statistical Library*, Version 2.0, IMSL Inc., Houston, September, 1991.
- [136] R. Bellman, R. Kalaba, and M. Prestrud, *Invariant Imbedding and Radiative Transfer in Slabs of Finite Thickness*, American Elsevier, N.Y., 1963.
- [137] M.E. Riley, Ph.D. Thesis, California Institute of Technology, Pasadena, CA, 1968.
- [138] W.H. Press, B.P. Flannery, S.A. Teukolsky, and W.T. Vetterling, *Numerical Recipes*, Cambridge Univ. Press, Cambridge, 1986.